Solar radiometer sensing of multi-year aerosol features over a tropical urban station: Direct Sun and inversion products

Katta Vijayakumar[1], Panuganti C. S. Devara[2*], Sunil M. Sonbawne[3], David M. Giles[4,5], Brent N. Holben[5], Sarangam Vijaya Bhaskara Rao[1]and Chalicheemalapalli K. Jayasankar[1]

[1] Department of Physics, Sri Venkateswara University (SVU), Tirupati 517502, India
[2] Amity Centre for Ocean-Atmospheric Science and Technology (ACOAST); Amity Centre for Environmental Science and Health (ACESH) &Amity School of Earth and Environmental Sciences (ASEES), Amity University Haryana, Manesar-Gurugram, 122413, India
[3] Indian Institute of Tropical Meteorology (IITM), Pune 411008, India
[4] Science Systems and Applications (SSA), Inc., Lanham, MD 20706, USA
[5] NASA Goddard Space Flight Center (GSFC), Greenbelt, MD 20771, USA

**Correspondence to*: P.C.S. Devara (pcsdevara@ggn.amity.edu)

Abstract. The AErosol RObotic NETwork (AERONET) is the most developed ground-based network for aerosol remote-sensing and has been playing a significant role not only in monitoring air quality for protecting human health but also in assessing the radiative budget of our planet Earth. In this paper, we report the direct sun and inversion products, comprising of spectral variation of Aerosol Optical Depth (AOD), associated Ångström Exponent (AE), fine- and coarse-mode aerosol fractions, Aerosol Size Distribution (ASD), Refractive Index (RI), Asymmetry Parameter (AP), Single Scattering Albedo (SSA), Aerosol Radiative Forcing (ARF), and columnar concentration of gas constituents such as water vapor (H_2O), obtained from a Cimel sun-sky radiometer, functioning at Pune, India, under the AERONET program since October 2004. These long-term measurements carried out from 2005 to 2015 could serve as an urban aerosol optical long-term average or climatology. The AOD long-term variations at all wavelengths, considered in the study, exhibited increasing trend, implying year-to-year enhancement in aerosol loading. The mean seasonal variations in AOD from cloud-free days indicated greater values during monsoon, revealing dominance of hygroscopic aerosol particles over the station. Contribution by different aerosol types to AOD has also been deduced, discussed and found dominance of mixed type of aerosols (44.85%), followed by combination of biomass burning and urban industrial aerosols (22.57%) compared to other types of aerosols during the study period. The long-term data sets, derived aerosol and trace gas products play a significant role in understanding aerosol climate forcing, trends, and evaluation of regional air pollution and validation of aerosol transport models over the study region.

1 Introduction

Atmospheric aerosol concentration and optical properties are one of the largest sources of uncertainty in current assessments and predictions of global climatic change (Hansen et al., 2000; IPCC, 2001). Changes in the aerosol content of the atmosphere constitute a major forcing mechanism by affecting the radiative balance of the climate system (Crutzen and Andreae, 1990; Charlson et al., 1992). A thorough understanding of regionally dependent chemical and optical properties of aerosols (e.g. aerosol optical thickness, size distribution) and their spatial (both horizontal and vertical) and temporal distribution is required for accurate evaluation of aerosol effects in the climate system (Hsu et al., 2000). Systematic observational evidence is required to study the highly variable characteristics of atmospheric aerosols in time and space (IPCC, 2007). Added, long-term measurements of key aerosol optical properties are urgently needed to better understand the climate changes (Wang et al., 2001; Streets et al., 2009; Wild et al., 2009). Aerosol optical depth (AOD) data from the Advanced Very High-Resolution Radiometer (AVHRR) satellite were used to account for the dimming and brightening tendencies (Mishchenko et al., 2007a; Zhao et al., 2008). Long-term aerosol datasets with climate quality is essential in reducing the uncertainty of aerosol effects on climate. Hence, there is an immediate need to regularly monitor aerosol distributions annually and seasonally, and to find out if there is any significant trend in their changing patterns over the years and what effect they will ultimately have on the regional/global climate. Such results greatly help in better quantification of aerosol radiative effects, aerosol–climate interactions and impacts of aerosol loading on the Earth's bio-geo-sphere.

Ground-based and space-borne optical remote sensing techniques are the most efficient means of studying aerosol particle parameters, properties, dynamics and lifetimes in the Earth's atmosphere due to local and global climate changes (King et al., 1999; Mishchenko et al., 2007b). The AErosol RObotic NETwork (AERONET; http://aeronet.gsfc.nasa.gov/), a ground-based remote sensing aerosol network of well-calibrated Sun/sky radiometers established in the early 1990s, is one of the well-developed and productive facility for passive aerosol measurements (Holben et al., 1998). Moreover, it is a well-established monitoring ground-based remote sensing aerosol network that is composed of more than 700 stations across the world. It provides standardized high-quality aerosol products (Xia, 2015) and the network continues to expand rapidly, which constitutes a valuable source of information for the establishment of local and regional aerosol characterizations (Holben et al., 2001). Further, AERONET provides continuous

time series data with a very high temporal resolution for the measurement sites over many years. These datasets have been used to obtain aerosol particle properties as a function of time in atmosphere column over the place and for satellite data validation (e.g., Abdou et al., 2005; Kacenelenbogen et al., 2006; Sinyuk et al., 2007). Coordination between surface-based network observations and satellite measurements are essential to develop a long-term monitoring system of the Earth's aerosol environment. The present communication deals with such a long-term dataset composed of direct sun products, covering from 2005 through 2015, archived at a site located in a tropical urban environment in central India.

2 Site description

Long-term aerosol data were acquired at a tropical urban site, Pune (18°32' N, 73°51' E, 559m above mean sea level), India as shown in Fig. 1. Pune is governed by Municipal Corporation which comes under Pune metropolitan region. Pune is the eighth largest metropolis in India and second largest in the state of Maharashtra (Source: https://pune.gov.in/). It is situated on the lee-side of the Western Ghats and is about 100 km inland from the west coast of India. In recent years, Pune has witnessed a substantial growth in terms of population as well as vehicular density and industrial installation due to rapid urbanization. Population of the Pune city is 31,32,143 as per 2011 census (Source: https://pmc.gov.in/en/census). The city is situated centrally between the other metropolises of Mumbai and Bangalore, and is well connected by road, rail and air. Observations were carried out on the terrace of the building at about 12 m above the surface. The site is surrounded by hillocks of variable height (up to 200 m), forming a valley-like terrain. The climate of the region is urban with a total rainfall of ~700 mm occurring mostly during the monsoon season in the June–September period and July is the wettest month of the year. The climatology of the area experiences four dominant seasons each year, pre-monsoon (March–May), monsoon (June–September), post-monsoon (October–November) and winter (December–February). The weather during pre-monsoon season is very hot with mostly gusty surface winds, and the daytime temperature reaches over 40° C. The air flow in the lower troposphere is predominantly westerly during the south-west (SW) monsoon season, which brings large influx of moist air from the Arabian Sea. The westerly flow sets in during the post-monsoon season, and rich continental air masses pass over the region during this season. Fair-weather conditions, with clear sky and very low relative humidity exist during the winter season. Low-level inversions during morning and

evening hours, and dust haze during morning hours, occur during this season. More details can be found in Devara et al. (1994; 2005).

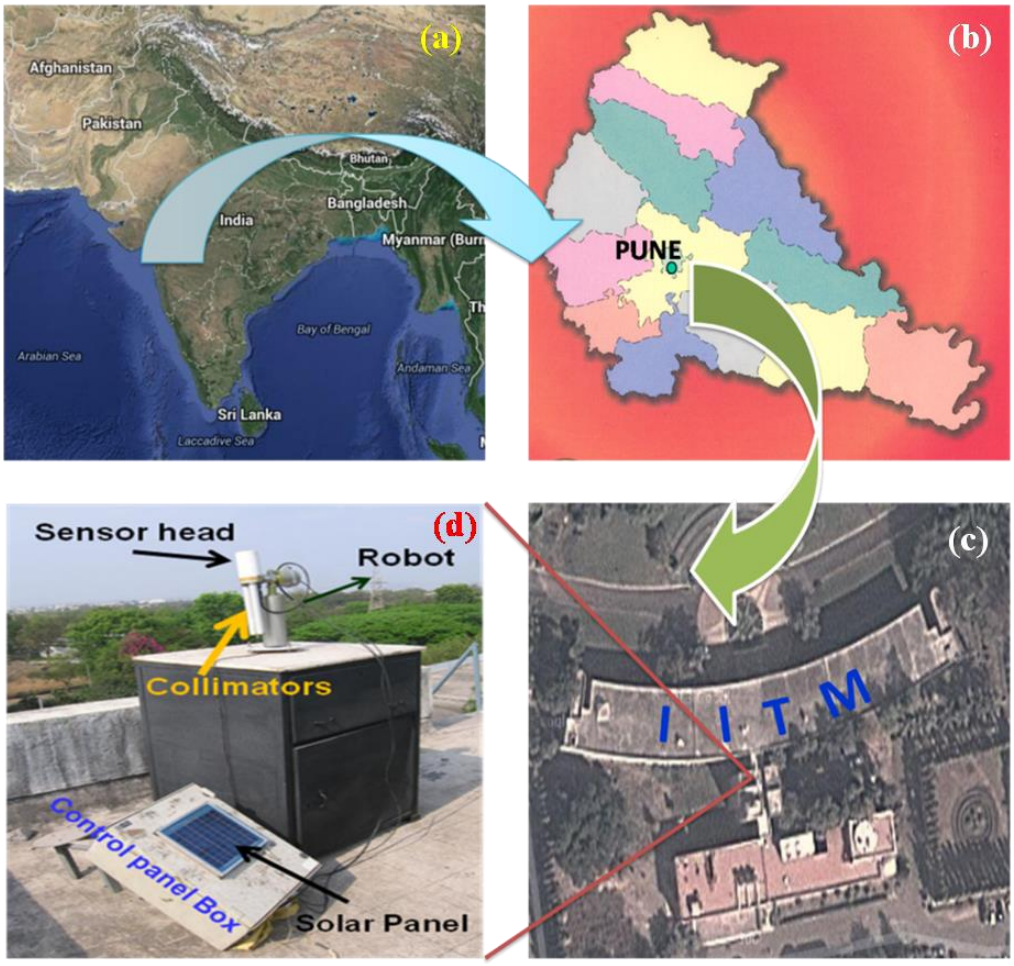

Figure 1. Location of Cimel Sun-Sky Radiometer, and its surroundings at Indian Institute of Tropical Meteorology (IITM), Pune (18° 32' N, 73° 51' E, 559m amsl), Maharashtra State, India. (Note: Figure 1(a) and (c) - base map from Google Earth, Source: https://earth.google.com. Figure 1(b) - base map from Google images of Maharashtra State map, Figure 1(d) - Radiometer with mount, and Control Panel Box with Solar Panel on its top).

3 Variations in meteorological elements

The meteorological key fields such as wind, temperature and humidity play vital role in several stages of aerosol optical, microphysical and dynamical evolution. In order to examine these

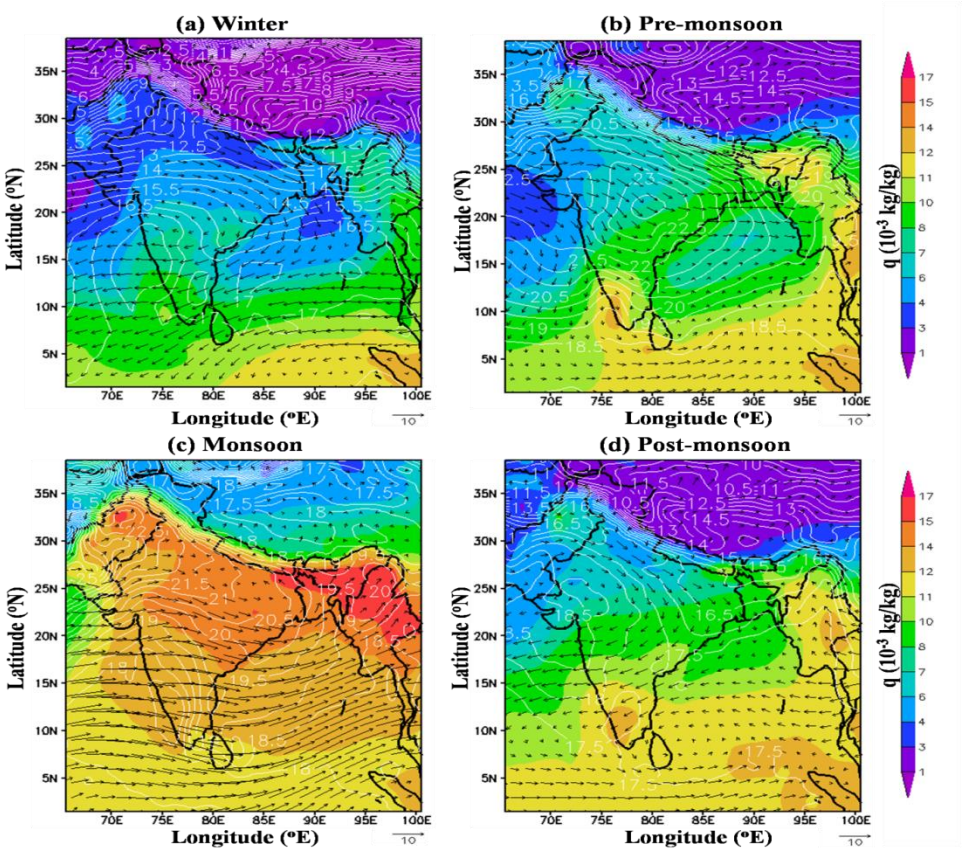

Figure 2. Seasonal composite of ECMWF wind, temperature and humidity fields over India during 2005–2015.

effects, European Centre for Medium-Range Weather Forecasts (ECMWF) reanalysis daily data for the study period, are shown in Fig. 2 (a: Winter; b: Pre-monsoon; c: Monsoon; d: Post-monsoon and wind, air temperature and specific humidity (q) at 850 hPa pressure level, averaged over the Indian region). Winds are represented with arrows pointing toward wind direction, where length and orientation of each arrow defines the magnitude (ms^{-1}) and direction (degrees), respectively. Line contours represent air temperature ($^{\circ}C$) and shaded color contours represent specific humidity/water vapor mixing ratio ($kg\ kg^{-1}$). It is evident from the figure that besides a large contrast between land and ocean regions, a significant seasonal variation in the above-mentioned parameters can be noted over the experimental site. Higher specific humidity values are evident over the Indo Gangetic Plain and ocean regions during monsoon season as compared to other three seasons. Highest moisture (q) values can be noted over the northern part of India during the monsoon season for the entire study period. In contrast, lowest q values can be seen over India

during winter season. The circulation was intense in and around India during monsoon as opposed to other seasons. However, anti-cyclonic circulation can be seen over India during winter and post-monsoon seasons while the winds were mostly north-westerly during pre-monsoon and south-westerly during monsoon during the study period. This would further be accentuated by the absence of rainfall, so that typical lifetime of aerosols is longer than ~1 week in the lower troposphere. These features favor growth and intrusion of aerosol particles from longer distances to the study site, which result in greater AOD values during monsoon season.

4 Instrumentation and data methodology

4.1 AERONET

All the ground-based measurements reported in this paper were made with CIMEL Electronique CE-318 sun/sky radiometer, which is a part of the AERONET global network. This instrument works on the principle of measuring the solar radiation intensity at some specified wavelengths and converts them into optical depth by knowing the corresponding intensities at the top-of-the-atmosphere (Holben et al., 1998). The CIMEL sun photometer is a solar-powered, hardy, robotically pointed sun and sky spectral radiometer. A microprocessor computes the position of the sun based on time, latitude, and longitude, which directs the sensor head to within approximately 1° of the sun, after which, a four-quadrant detector tracks the sun precisely to a programmed measurement sequence. After the routine measurement is completed, the instrument returns to the "park" position, awaiting the next measurement sequence. A "wet sensor" exposed to precipitation will cancel any measurement sequence during rain events. Data in the memory of the sun photometer are transferred to the PC and are sent to NASA for processing and archival of products. The columnar precipitable water content is determined based on the measurements at 940 nm (H_2O absorption peak) and at 1020 nm (no absorption by water content). The details of the retrieval of water content and the types of errors involved in it can be found in the works of Schmid et al. (2001), Devara et al. (2001), Smirnov et al. (2004) and Alexandrov et al. (2009). The scenario, 'Almucantar' denotes a series of measurements taken at an elevation angle of the Sun for specific azimuth angles relative to the position of the Sun. These measurements are taken at 440, 675, 870 and 1020 nm channels. During almucantar measurements, observations from a single channel are made in a sweep at a constant elevation angle across the solar disc and continue $\pm 180^{\circ}$ from the Sun in

about 40s. This is repeated for each channel to complete an almucantar sequence (Holben et al., 1998).

The calibration of the instrument was performed regularly at the Goddard Space Flight Center (GSFC) by a transfer of calibration from reference instruments that were calibrated by the Langley method at Mauna Loa Observatory (MLO), Hawaii. The combined effects of uncertainties in calibration, atmospheric pressure, and total ozone amount (climatology is used) result in a total uncertainty in derived aerosol optical depth of ~0.010-0.021, with the largest error in the UV (Eck et al., 1999). The AERONET algorithms compute the aerosol optical depth retrievals in near real time (Holben et al., 1998). Data are quality checked and cloud-screened following the methodology of Smirnov et al. (2000), which relies on the greater temporal variance of cloud optical depth versus aerosol optical depth. The AERONET archive is divided into 3 quality levels: level 1.0 for raw data, level 1.5 for cloud-screened data and level 2.0 for quality assured data (Holben et al., 1998; Smirnov et al., 2000) and can be downloaded from the AERONET website (http://aeronet.gsfc.nasa.gov/). The AERONET data (from January 2005 to December 2015) used in this study belong to version 2.0 at level 2.0, which are cloud-screened and have been manual screening, ensuring the data quality (Giles et al., 2019). A number of studies have already described the instrumentation, data acquisition, retrieval algorithms, and calibration procedures, which conform to the standards of the AERONET global network, as well as the uncertainty in final products and the applied cloud-screening procedures (Holben et al., 1998; 2001; Eck et al., 1999; Smirnov et al., 2000, 2002a, 2002b). More details about AERONET instrument used in the present study at Pune, India have been reported by Kumar et al. (2011).

4.2 Estimation of ARF

In the present study, the aerosol radiative forcing (ARF) at BOA, ATM and TOA has been estimated by following the method reported by Xie et al. (2018). This method involves forcing calculations from broadband fluxes between 0.2 and 4.0 micron from aerosol size distribution, spectral AOD, single scattering albedo and phase function by using the radiative transfer module integrated in the AERONET inversions (Garcia et al., 2008; 2012). In this method, the AERONET-defined RF_{TOA} and RF_{BOA} have been directly used to calculate $RF_{ATM} = RF_{TOA} - RF_{BOA}$.

4.3 MODIS

The Moderate-resolution Imaging Spectroradiometer (MODIS) is a scientific instrument (radiometer) on board the NASA Terra and Aqua satellite platforms. Both Terra and Aqua satellite platforms, launched in 1999 and 2002 respectively to study global dynamics of the Earth`s atmosphere, land, ice and oceans. Thus, the instrument collects a variety of global data sets. Terra and Aqua satellites with MODIS instruments attached fly on the sun-synchronous orbits at 705km altitude and pass over the same spot of the Earth at about the same local time every day, i.e., 10:30AM in the case of Terra and 1:30PM for Aqua. Due to the large swath of data collected by MODIS (over 2300 km wide) it is possible to observe almost the entire Earth surface every day. MODIS measures reflected solar and emitted thermal radiation in a total of 36 bands ranging in wavelength from 0.4 µm to 14.4 µm and at varying spatial resolutions (2 bands at 250 m, 5 bands at 500 m and 29 bands at 1 km). Detailed descriptions of the MODIS aerosol retrieval and its evolution since the start of MODIS operation are given in the work of Remer et al. (2005). In this study, deep blue product of AOD at 550nm and water vapor observation used.

4.4 OMI

The Ozone Monitoring Instrument (OMI) measures the solar radiation backscattered by the Earth's atmosphere and surface over the entire wavelength range from 270 to 500 nm with a spectral resolution of about 0.5 nm. OMI measurements are highly synergistic with the other instruments on the Aura platform. The 114° viewing angle of the telescope corresponds to a 2600 km wide swath on the surface, which enables measurements with a daily global coverage. OMI continues the TOMS record for total Ozone and other atmospheric parameters related to Ozone chemistry and climate. Also, total columns of gases like NO_2, BrO and SO_2 will be derived. The US Environmental Protection Agency (EPA) has designated these atmospheric constituents as posing serious threats to human health and agricultural productivity. These measurements are made at near urban scale resolution and track industrial pollution and biomass burning. Furthermore, aerosol and cloud parameters will be determined from the OMI measurements. The OMI instrument is a contribution of the Netherlands's Agency for Aerospace Programs (NIVR) in collaboration with the Finnish Meteorological Institute (FMI) to the Aura mission. In this study, we used OMAEROev003 product of AOD at 442nm measurements for comparison with ground-based observations of AERONET data during study period.

4.5 Heating rate

The amount of solar radiation trapped in the atmosphere by aerosols, as quantified by the atmospheric heating rate (HR; $Kday^{-1}$), has been analyzed. The HR due to aerosol absorption is calculated according to the first law of thermodynamics and assuming hydrostatic equilibrium, as suggested by Liou (2002):

$$\frac{\partial T}{\partial t} = \frac{g}{Cp}\frac{ARF_{ATM}}{\nabla P}$$

Where $\frac{\partial T}{\partial t}$ is the HR in $Kday^{-1}$, g is the acceleration due to gravity, C_P is the specific heat capacity of air at constant pressure (i.e., ~1006 J $kg^{-1}K^{-1}$), and ∇P is the atmospheric pressure difference between surface and 3 km altitude, where most aerosols are present.

4.6 Discrimination of aerosol types

The discrimination of aerosol types increases accuracy of the assessment of the aerosol radiative impact and therefore, is important to climate modeling (Diner et al., 1999). Previous studies showed that different aerosol types have different effects on climate because their diverse morphology, size distribution, hygroscopic properties, and chemical component will lead to different aerosol optical properties (Giles et al., 2011; 2012; He et al., 2018; Kumar et al., 2018). For example, dust aerosols are often large particles and have a scattering tendency (Vijayakumar et al., 2014), whereas black carbon aerosols are usually smaller particles and have an absorbing nature (Tan et al., 2016). Various optical and microphysical parameters have been used for aerosol classification. The spectral dependence of aerosol optical depth (AOD), expressed by the Angstrom Exponent (AE), is a good indicator of particle size. These two parameters are commonly used in aerosol remote sensing to infer dominant aerosol types given knowledge of the source region or typical aerosol transport mechanisms (Kaskaoutis et al., 2009; Pathak et al., 2012; Vijayakumar and Devara, 2013; Verma et al., 2015). Gobbi et al. (2007) used this parameter and its spectral curvature to propose a graphical method for evaluating the contribution of fine mode particles to AOD and to track mixture of pollution containing dust. Schuster et al. (2006) determined that variation in AE wavelength pairs is sensitive to aerosol composition. In addition, the spectral AOD and AE data was used in deriving the curvatures (a_1 and a_2) correlated with AOD can be effectively used for discriminating different aerosol types (Vijayakumar et al., 2012; Kumar et al., 2013) information content from these relationships varies from generic identification of

major aerosol particle types (e.g., dust mixed and urban/industrial pollution) to specific degrees of absorbing aerosols. In the Indian subcontinent, Kaskaoutis et al. (2009) have made the first attempt to distinguish different aerosol types originating from variety of sources over Hyderabad. Furthermore, Vijayakumar et al. (2012) over Pune and Vijayakumar and Devara, (2013) over Sinhagad have discriminated different aerosol types over different regions in the Indian landmass.

For the classification of aerosols into specific types some "appropriate" threshold values are required. Our approach to infer major aerosol types is based on the combination of particle size and absorption/scattering information, following Kaskaoutis et al. (2009), Vijayakumar et al. (2014) and Lee et al. (2010). The AOD-AE patterns have been utilized to describe different aerosol types (e.g., Clean maritime, Continental clean, Desert dust, Urban industrial/Biomass burning and Mixed type aerosol). In this study we used AOD at 440nm and Angstrom exponent is 440-870nm. The threshold values, used in this study represented a slight adjustment from those previously used authors, as cited above. Cases of $AOD_{440nm} < 0.2$ with $AE_{440\text{-}870nm}$ values of small (< 0.9) or large (> 1.0) represented clean maritime-influenced aerosols (CM) and continental clean type represented as background aerosols (CC), respectively. $AOD_{440nm} > 0.3$ and $AE_{440\text{-}870nm} > 1.0$ can be used to characterize long-range transported biomass burning/urban industrial aerosols (BB/UI), and AOD_{440nm} values > 0.6 associated with $AE_{440\text{-}870nm}$ values < 0.7 are indicative of desert dust (DD) particles transported over oceanic areas. Finally, where the aerosols are difficult to be discriminated and they are considered as mixed aerosol type (MA), bearing in mind, the different effects of various aerosol-mixing processes in the atmosphere (e.g., coagulation, condensation, humidification, gas-to-particle conversion). The classification method (AOD_{440nm} Vs. $AE_{440\text{-}870nm}$) is illustrated in Fig. 3(a).

CIMEL sun/sky radiometer derived fine-mode fraction (FMF) at 500nm has been used to represent the dominant aerosol size mode, because FMF provides quantitative information for both fine- and coarse-mode aerosols. SSA has been used to quantify the aerosol absorption/scattering at 440nm, which is the shortest wavelength of AERONET channels and generally used to distinguish absorbing from non-absorbing aerosols (Lee et al., 2010). The categories of aerosol types are distinguished between FMF_{500nm} and SSA_{440nm} is polluted dust (PD, dominantly dust with anthropogenic aerosols), polluted continental (PC, dominantly anthropogenic mixed with dust), absorbing and non-absorbing aerosols. The threshold values of groups are as follows: (i) $FMF_{500nm} < 0.4$ for any range of SSA_{440nm} indicates predominantly coarse mode aerosols and hence

assigned to polluted dust (PD), (ii) introducing a safety margin of 0.4 between fine- and coarse-mode aerosol, $0.4 \leq FMF_{500nm} \leq 0.6$ for any range of SSA_{440nm} represented polluted continental (PC). All $FMF_{500nm} > 0.6$ were considered as fine-mode aerosols which were further discriminated as absorbing (mainly black carbon, BC) or non-absorbing depending on values of SSA440. (iii) $FMF_{500nm} > 0.6$ with $SSA_{440nm} > 0.95$ as non-absorbing (NA, which includes sulfates, nitrates and aged water-soluble organic carbons), (iv) $FMF_{500nm} > 0.6$, $0.90 < SSA_{440nm} \leq 0.95$ as slightly-absorbing (SA), (v) $FMF_{500nm} > 0.6$, $0.85 < SSA_{440nm} \leq 0.90$ as moderately-absorbing (MA), whereas (vi) $FMF_{500nm} > 0.6$ with $SSA_{440nm} \leq 0.85$ represented highly-absorbing (HA) fine-mode aerosols. It should be noted that this classification must be considered only qualitatively not quantitatively, since the percentages may be strongly modified with a change in the AOD_{440nm}, $AE_{440\text{-}870nm}$, FMF_{500nm} and SSA_{440nm} threshold values. The method of classification (SSA_{440nm} Vs. FMF_{500nm}) is illustrated in Fig. 3(b).

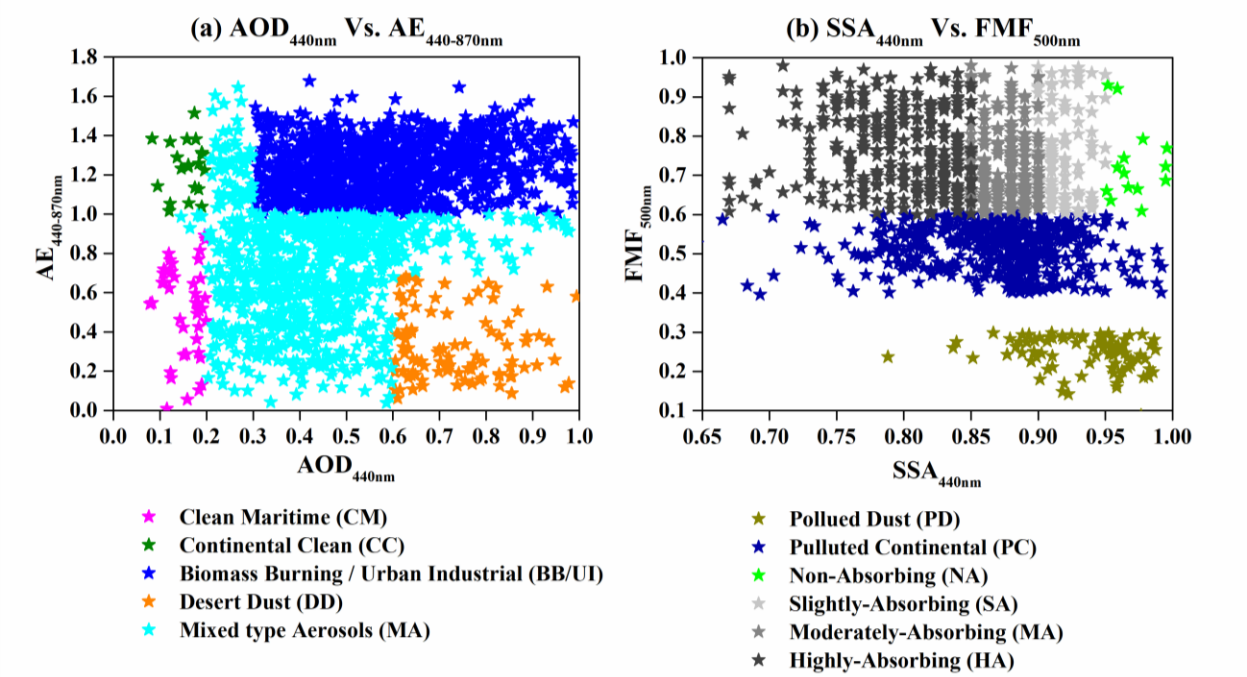

Figure 3. Classification of aerosol types based on different thresholds of (a) AOD_{440nm} Vs. $AE_{440\text{-}870nm}$, and (b) SSA_{440nm} Vs. FMF_{500nm}.

5 Results and discussion

When making ground-based observations at single point, it is important to know their representativeness for the region under consideration. Long-term monitoring of aerosol optical properties over Pune AERONET site was performed, on all non-rainy days, from January 2005 to December 2015. The distribution of the number of observations in each month during the study period (one decade) is shown in a bar diagram (Fig. 4). The month-to-month variation in number of observation days, and data gaps in the data series are due to unfavorable sky conditions over the study site, and due to shipment of the instrument for calibration at, GSFC, NASA, USA.

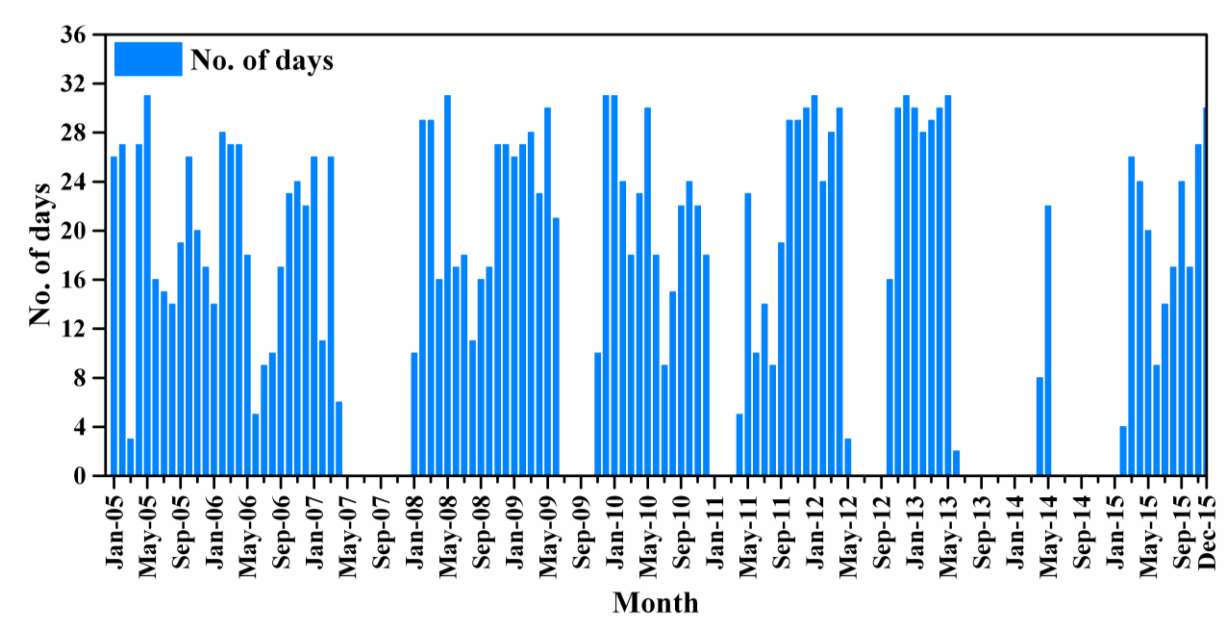

Figure 4. Month-wise distribution of observation days during the study period from January 2005 through December 2015.

5.1 Aerosol optical depth (AOD)

Aerosols originating from differing source regions are likely to have significant differences in their optical properties. However, regional distribution of aerosols, their inter-annual variability and detailed description of spectral aerosol optical properties are needed to understand the influence of aerosols on the climate of the study region (Eck et al., 2001). The optical properties of aerosols over Pune (one of the rapidly growing cities) show strong seasonal and inter-annual variations. Aerosol characteristics vary with time and region because of its different aerosol sources (e.g.

aerosol types and emission intensity) and different atmospheric conditions (e.g. relative humidity and boundary layer height etc.). The Cimel sun-sky radiometer of AERONET, used in the present study, provides the column-integrated aerosol optical depth at different wavelengths. Such columnar optical depth is appropriate for most of the radiative forcing assessments. Figure 5 depicts the composite picture of spectral variation of AOD for the entire observation period from January 2005 to December 2015. While the maximum AOD value 0.52 at 440 nm and minimum value of 0.28 at 1020 nm, it shows strict wavelength dependence (higher AOD at shorter wavelength and vice-versa).

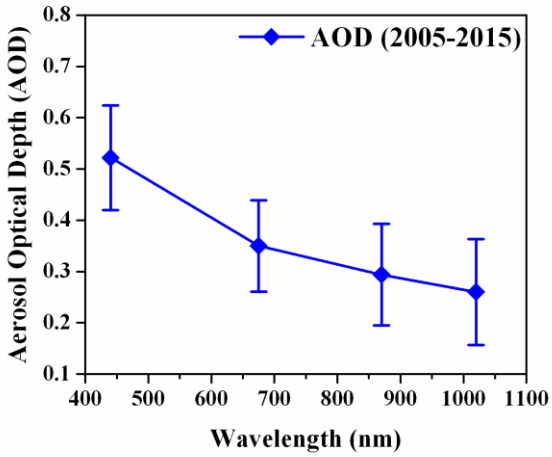

Figure 5. Composite spectral AOD variations from one-decade Cimel measurements at Pune, India. Vertical bar at each data point represents standard deviation from mean.

5.2 Aerosol Size Distribution (ASD)

The size distribution of aerosols is an important parameter in understanding their climate effect. The world-wide aerosol size distribution exhibits two distinct modes: fine particles with particle size <0.6 μm and coarse with particles size >0.6 μm (Dubovik et al., 2002). So, the fine and coarse modes can be separated by a radius of ~0.6 μm. The bimodal structure of volume size distribution may be due to various reasons, such as mixing of two air masses with different aerosol populations (Hoppel et al., 1985), homogeneous hetero-molecular nucleation of new fine particles in the air, or heterogeneous nucleation and growth of large particles by condensation of gas-phase products. The AERONET aerosol size distributions are retrieved from the spectral sun photometer using 22 radius size bins in the size range of 0.05-15 μm. Figure 6 shows the composite volume size distribution of aerosols over Pune. Here r_{min} and r_{max} shows range of radii for corresponding

modes. The value of volume size distribution in coarse-mode is higher compared to fine-mode due to likely to be caused by atmospheric elements.

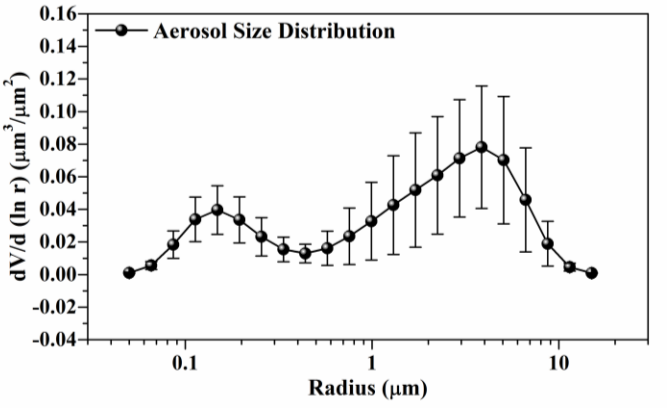

Figure 6. Composite volume size distribution of aerosols over Pune during 2005-2015.

5.3 Effective radius (R_{eff}) and volume-weighted mean radius (Rv)

The time series of monthly mean R_{eff} (for coarse-mode) and Rv (for fine -mode) are shown in Fig. 7. Both parameters show slightly decreasing trend by 0.13% per year for effective radius and increased trend by 2.14% per year for volume weighted mean radius due to lack of observations and unfavorable sky conditions.

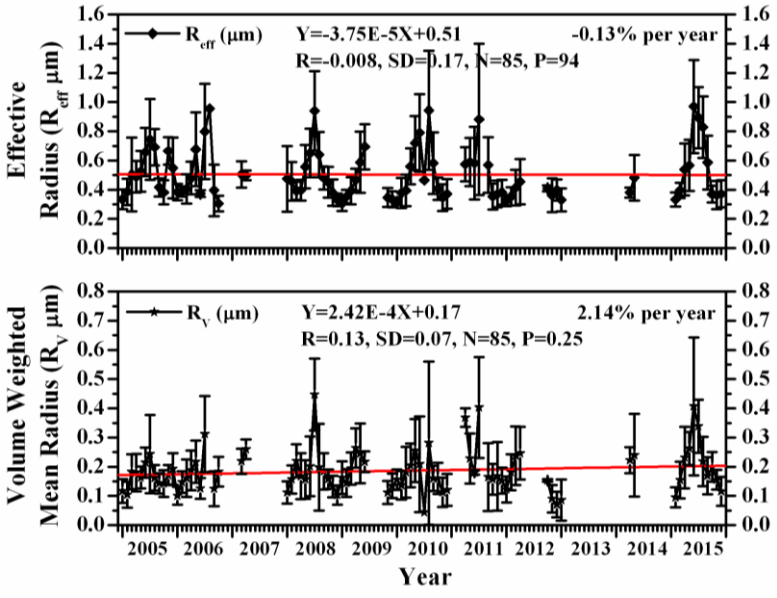

Figure 7. Long-term monthly mean variation of Effective radius (R_{eff}μm) and Volume weighted mean radius (R_vμm). Vertical bar at each data point represents standard deviation from mean.

5.4 Aerosol radiative forcing (ARF)

Aerosols modify incoming solar and outgoing infrared radiation. The aerosol radiative forcing (ARF) at the top of the atmosphere (TOA) or at the bottom of the atmosphere (BOA) is defined as the difference in the net solar fluxes (down minus up) (solar plus long wave; in Wm^{-2}) with and without aerosol. The difference between these two quantities gives the ARF in the whole atmosphere. Generally, negative values of TOA, implying the presence of aerosols results in increase in the radiation loss to the space (by enhanced backscattering) leading to a cooling in the earth-atmosphere system, while positive value imply an atmospheric warming. At the bottom (surface), the BOA forcing will always be negative because aerosols reduce the surface reaching solar radiation and these values are more sensitive to aerosol loading only. The difference between the radiative forcing at TOA and BOA is defined as atmospheric forcing (ATM). It represents the amount of energy trapped within the atmosphere due to the presence of aerosols. If ATM is positive the aerosols produce a net gain of radiative flux to the atmosphere leading to a heating (warming), while negative ATM indicates loss and thereby cooling. Generally, the intensity of ARF depends on the aerosol loading, and therefore it is difficult to consistently inter-compare the radiative forcing by the typical aerosol types. Seasonal variations of radiative forcing at TOA, BOA and ATM observed in the present study are compared with such studies available at other Indian sites in Table 1.

Table 1. Comparison of Aerosol Radiative Forcing (Wm^{-2}) at different stations in India.

Stations (Latitude, Longitude, amsl)	Seasons	Aerosol Radiative Forcing (Wm^{-2})			Reference
		TOA	BOA	ATM	
Delhi (28.63°N, 77.17°E, ~235m amsl)	Pre-monsoon	–3.6	–69.6	+198.0	Pandithurai et al., 2008
Dibrugarh (27.3°N, 94.6°E, ~111m amsl)	Pre-monsoon	–1.4	–37.1	+35.7	Pathak et al., 2010
	Monsoon	–1.5	–33.7	+32.2	
	Post-monsoon	–	–12.5	+12.6	
	Winter	–1.0	–34.2	+33.2	
Bangalore (13°N, 77°E, ~960m amsl)	November	+5.0	-23.0	+28.0	Babu et al., 2002

Hyderabad (17.38°N, 78.45°E, ~515m amsl)	Pre-monsoon	-25.5	-128.4	+102.8	Sinha et al., 2012
	Monsoon	-34.2	-112.9	+78.6	
	Post-monsoon	-21.8	-110.5	+88.6	
	Winter	-21.4	-144.5	+123.0	
Kanpur (26.47°N, 80.33°E, ~142m amsl)	Pre-monsoon	–12.8	–57.0	+44.2	Kaskaoutis et al., 2013
	Monsoon	–17.1	–42.5	+25.4	
	Post-monsoon	–17.6	–47.0	+29.5	
	Winter	–14.5	–49.1	+34.6	
Chennai (12.81°N, 80.03°E, ~45m amsl)	Pre-monsoon	+5.8	–32.5	+38.3	Aruna et al., 2016
	Monsoon	–6.0	–38.4	+32.4	
	Post-monsoon	–4.3	–32.3	+27.9	
	Winter	+5.4	–35.3	+40.7	
Trivandrum (8.55°N, 76.97°E, ~3m amsl)	Pre-monsoon	+0.3	–35.8	+35.2	Babu et al., 2007
	Monsoon	–2.0	–25.7	+23.7	
	Post-monsoon	–2.2	–29.0	+26.9	
	Winter	+2.9	–46.9	+49.8	
Ahmedabad (23.03°N, 72.55°E, ~50m amsl)	Pre-monsoon	+8.0	–41.4	+49.4	Ganguly et al., 2006
	Monsoon	+14.0	–41.0	+55.5	
	Post-monsoon	–22.0	–63.0	+41.0	
	Winter	–26.0	–54.0	+28.0	
Pune (18.32°N, 73.51°E, ~559m amsl)	Pre-monsoon	–20.6	–72.8	+58.4	
	Monsoon	–25.2	–62.2	+52.3	**Present study**
	Post-monsoon	–20.8	–76.8	+37.1	
	Winter	–14.8	–73.3	+55.9	

5.5. Columnar water vapor (CWV)

The year-to-year variation in columnar precipitable water content is shown in Fig. 8. A monotonic increase in water vapor at a rate of 1.16%Yr $^{-1}$ is evident from the figure. This feature provides additional support to attribute the increase observed in AODs that can occur because of hygroscopic growth of water-soluble aerosols, transport of larger sized aerosols (dust and sea salt) during favorable wind conditions (Ramachandran and Cherian, 2008) and new particle formation by condensation and nucleation, showing higher aerosol optical depths. The lower AOD values, observed in post-monsoon season, could be explained due to wet soil which inhibits aerosol emissions in the lower atmosphere.

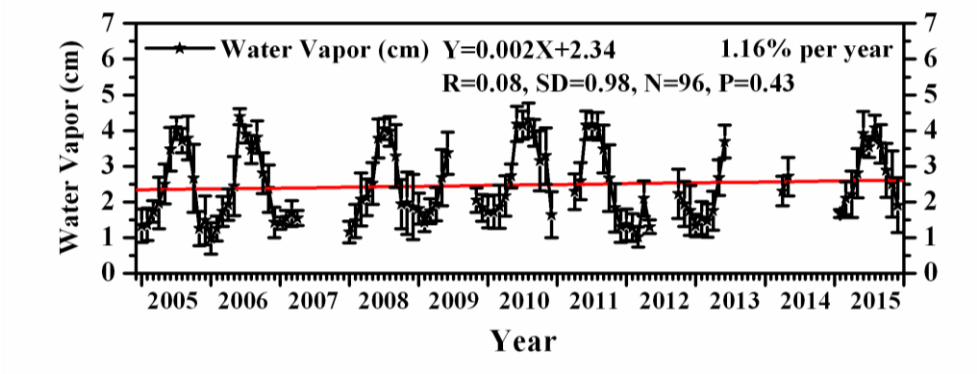

Figure 8. Monthly mean variations in columnar precipitable water content during 2005-2015 over Pune, India.

5.6 Ångström exponent (AE), fine- and coarse-mode AOD

Greater AE values during winter and post-monsoon seasons indicate rich concentration of fine-mode particles. The strong decrease in $\alpha_{440-870}$ value during the monsoon season could be explained based on coarse-mode particles originating from the Arabian Sea (Kumar et al., 2011). Thus, the decrease of α from winter to pre-monsoon, and monsoon months is indicative of increased coarse-mode particle contribution, consistent dust particles (>10 μm) in the aerosol loading. This strong decrease in $\alpha_{440-870}$ value could be due to mixing of air originating from oceanic and desert regions. The notable lower values of the Ångström Exponent during June-September are ascribed to be due to cloud contamination of data retrievals caused by thin invisible cirrus (Chew et al., 2011; Huang et al., 2012).

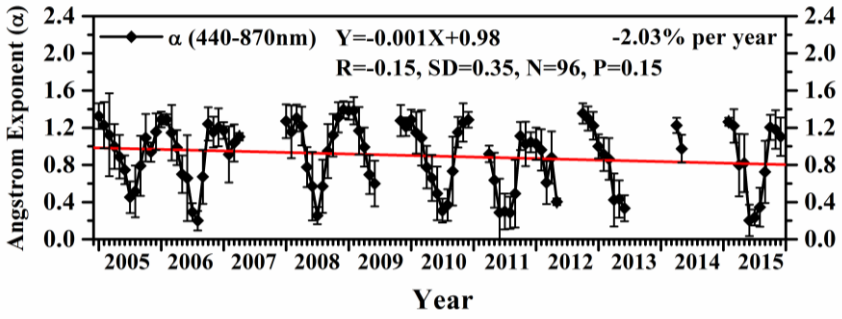

Figure 9. Monthly mean variation of Angstrom Exponent (AE) during the study period. Vertical bar at each data point represents standard deviation from mean. Solid red line indicates long-term decreasing trend.

Monthly averages of the Ångström exponent, $\alpha_{440-870}$ for the whole period of observations is shown in Fig. 9. The Ångström exponent appears to have decreased by about 2.03% per year over the duration of the study period. The monthly mean values of the Ångström exponent varied from 0.21 to 1.35, representing a minimum value in January (0.21±0.07) and maximum in July (1.35±0.07), which is consistent.

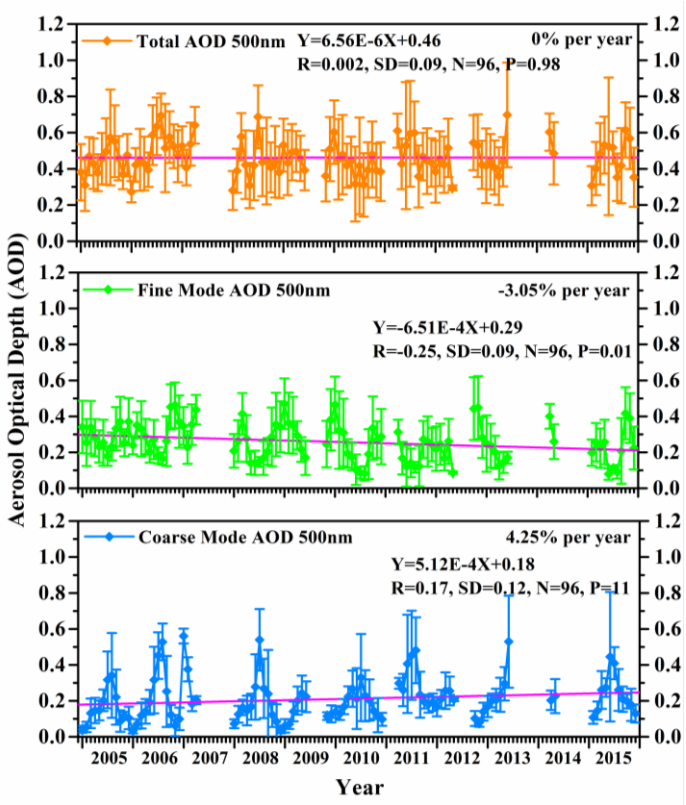

Figure 10. Year-to-year variation in total, fine-mode and coarse-mode AOD during 2005-2015. The solid red-color lines passing through the data represent respective long-term trends. Vertical bar at each data point represents standard deviation from mean.

The direct-Sun AOD measurements and almucantar scan inversions, the spectral deconvolution algorithm (SDA) applied to the direct-Sun AOD analysis to partition the fine- and coarse- mode contributions to the total AOD at a standard wavelength of 500nm (O'Neill et al., 2001, 2003). This parameter proves to be a quite effective indicator of the size distribution of the observed aerosols. Figure 10 displays the monthly mean variations of total, fine-mode and coarse-mode AOD at 500nm. It is evident that the total AOD is almost constant throughout period, while the fine-mode shows decreasing trend (-3.05% y^{-1}) and coarse-mode shows increasing trend

435 (4.25% y^{-1}). The decreasing trend in fine-mode implies reduction in anthropogenic activity while the increasing trend in coarse-mode suggests dominance of natural sources such as dust, sea-salt.

5.7 Seasonal variation of Aerosol Types

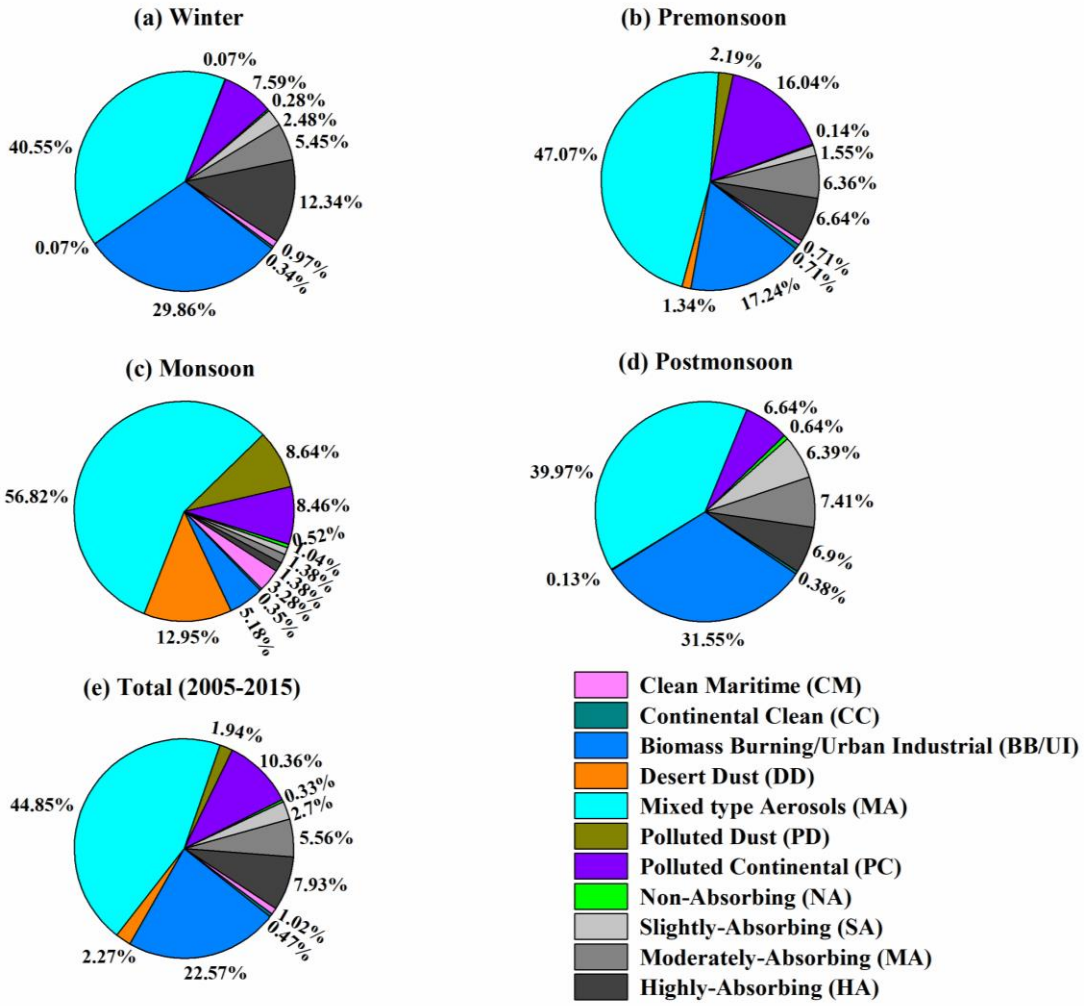

Figure 11. Average proportion of different aerosol types in (a) Winter, (b) Pre-monsoon, (c) Monsoon, (d) Post-monsoon, and (e) Total (2005-2015).

Figure 11 shows the pie diagram of different aerosol types over Pune using above threshold values. The analysis reveals that the MT aerosols clearly dominates in pre-monsoon (47.07%) and monsoon (56.82%) and in some fractions (40.55%, 39.97%) during winter and post-monsoon seasons, while the BB/UI type exhibits its highest presence during post-monsoon (31.55%) and

more rarely (5.18%) in monsoon season. It is interesting to note that CM aerosols are absent during post-monsoon period. Polluted continental aerosols are dominated in pre-monsoon (16.04%), compared to monsoon (8.46%) and post-monsoon (6.64%) due to rainout/washout effects.

The absorbing aerosols have very less contribution in monsoon season. Overall, the MT (44.85%) aerosols are dominated compare to other type of aerosols over study region. Furthermore, the total contribution of various types of aerosols is CM (1.02%), CC (0.47%), BB/UI (22.57%), DD (2.27%), PD (1.94%), PC (10.36%), SA (2.7%), MA (5.56%), HA (7.93%), and NA (0.33%). However, it should be noted that the present fractions may be considered rather qualitatively and not quantitatively, since they correspond to specific threshold values, while an alteration in the thresholds would have cause changes in the fractions, but not in the general pattern of the seasonal distribution of aerosol types. A comparison of the present results of Pune with those obtained from similar analysis performed over other locations in the Globe is not an easy task due to different land-use and environmental characteristics, differences in the time periods of the observations and in the seasonal pattern of the air masses and long-range transport, the specific influence of anthropogenic pollution etc. Similar analysis performed over other locations in the Globe is not an easy task due to different land-use and environmental characteristics, differences in the time periods of the observations and in the seasonal pattern of the air masses and long-range transport, the specific influence of anthropogenic pollution etc. The aerosol types inferred from the present study are compared with those obtained from other Indian sites in Table 2.

Table 2. Comparison of aerosol types at different stations in India.

Station (Latitude, Longitude, amsl)	Aerosol types	Percentage of different types of aerosols in different seasons				References
		Pre-monsoon	Monsoon	Post-monsoon	Winter	
Hyderabad (17.38°N, 78.45°E, ~515m amsl)	MI	0.5	7.1	8.7	2.6	Kaskaoutis et al., 2009
	MT	44.3	56.0	72.9	62.2	
	HUI	47.2	6.6	14.3	32.3	
	HDD	7.91	30.3	4.1	2.9	
Jaipur	BB	0.0	–	–	20.5	Verma et al., 2015
	AB	16.7	–	–	5.6	

(26.9°N, 75.8°E, ~450m amsl)	DD	48.9	–	–	0.0	
	MR	22.5	–	–	0.4	
	MT	11.7	–	–	73.5	
Varanasi (25.2°N, 82.9°E, ~83m amsl)	PC	40.0	23.0	1.0	3.0	Tiwari et al., 2018
	MT	25.0	21.0	4.0	12.0	
	AA	20.0	41.0	56.0	61.0	
	BB	3.0	2.0	37.0	22.0	
	MD	12.0	13.0	2.0	2.0	
Pune (18.32°N, 73.51°E, ~559m amsl)	CM	0.7	3.2	0.0	0.9	
	CC	0.7	0.3	0.3	0.3	**Present study**
	BB/UI	17.2	5.1	31.5	29.8	
	DD	1.3	12.9	0.1	0.07	
	MA	47.0	58.8	39.9	40.5	
	PD	2.2	8.6	0.0	0.07	
	PC	16.0	8.4	6.6	7.5	
	NA	0.1	0.5	0.6	0.2	
	SA	1.5	1.0	6.3	2.4	
	MA	6.3	1.3	7.4	5.4	
	HA	6.6	1.3	6.9	12.3	

Note: Where MI=Maritime Influenced; MT=Mixed Type; HUI=High AOD Urban/Industrial; HDD=High AOD Desert Dust; BB= Biomass Burning; AB=Arid Back ground; DD= Desert Dust; MR=Marine; PC=Polluted Continental; AA=Anthropogenic Aerosols; MD=Mostly Dust; CM=Clean Maritime; CC=Continental Clean; BB/UI=Biomass Burning/Urban Industrial; MA=Mixed type Aerosols; PD=Polluted Dust; NA=Non-Absorbing; SA=Slightly-Absorbing; MA=Moderately-Absorbing; HA=Highly-Absorbing.

5.8. Seasonal variation in Aerosol Products during 2005-2015

In order to obtain a holistic view of the regional aerosol characteristics during the period of study, the seasonal variations in aerosol quantities are grouped and shown in Fig. 12. The different panels in the figure display variations in different aerosol products. Different frames in this figure indicate variations in aerosol optical depth (Frame; a); water vapor (Frame: b); Angstrom Exponent (Frame: c); Total, fine-mode and coarse-mode fractions (Frame: d); aerosol size distribution (Frame: e); single scattering albedo (Frame: f); Asymmetry factor (Frame: g); aerosol refractive index, real (Frame: h); refractive index, imaginary (Frame: i); effective radius (Frame: j) and volume weighted mean radius (Frame: k).

Frame (a) displays the seasonal variation of AOD at different wavelengths. At all wavelengths, AODs show lower values in winter season which could be due to strong inversions, and whatever aerosols due to various human activities (domestic cooking, vehicular and industrial

emissions, etc.) are let out into the surface layer get trapped in the lower atmosphere due to less ventilation.

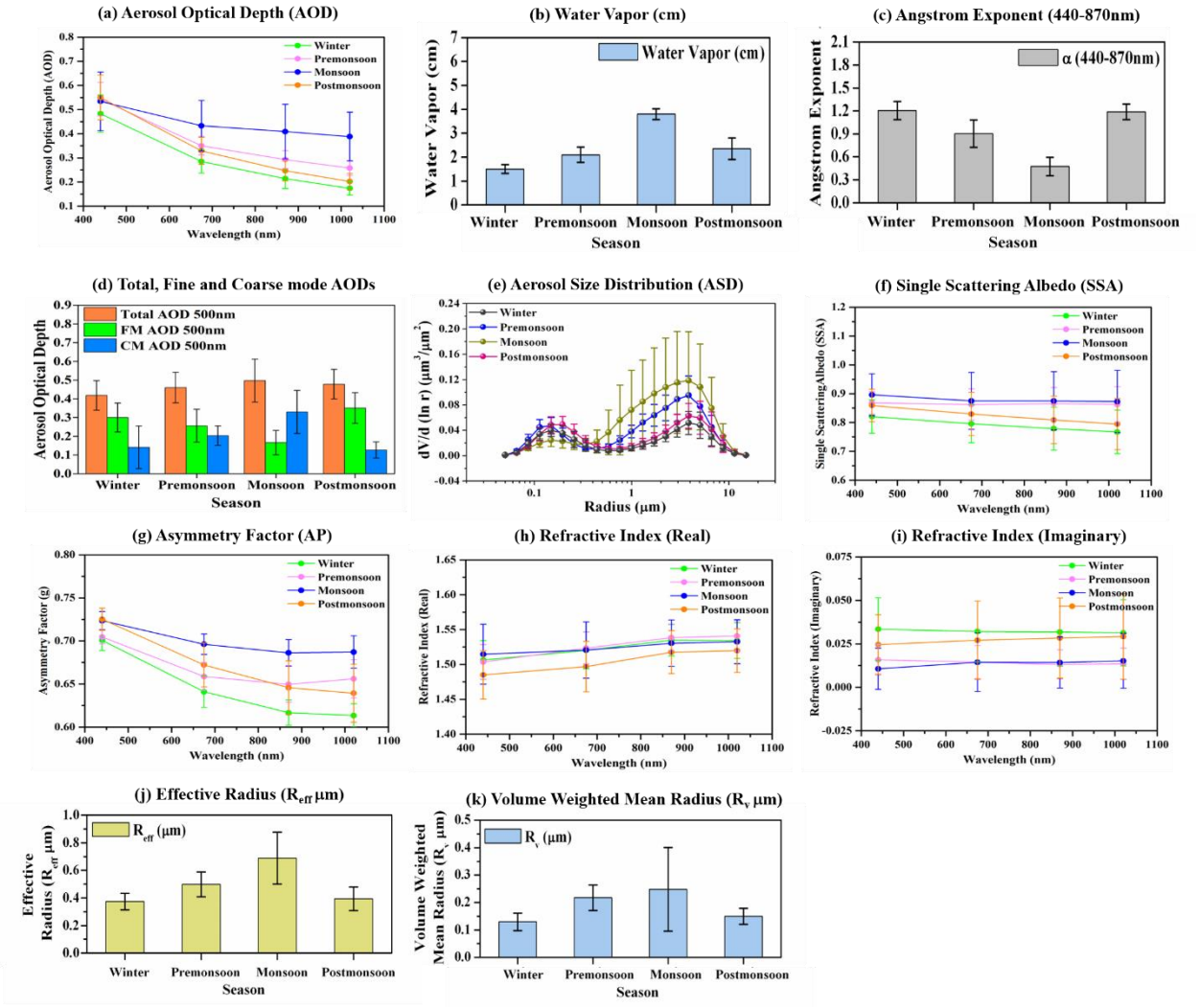

Figure 12. Seasonal mean variations in aerosol products.

Also, due to calm wind conditions, aerosols of soil-dust type are less during winter. In the pre-monsoon, the greater AOD values be attributed to the increased concentration of continental aerosol loading due to higher temperatures in the study region. Moreover, processes such as long-range transport are decreasing from winter to pre-monsoon which may be associated with air masses consisting of dust from west of the Arabian Sea (Devara et al., 2002; Kumar et al., 2011). In addition, Vijayakumar and Devara (2012) reported that the anthropogenic aerosols are abundant in pre-monsoon season could also be due to festive celebrations. In India, we celebrate a festival called 'HOLI' every year during the pre-monsoon season. More popularly, this festival is also

known as 'Festival of Colors'. During this festival, people play with colored powder and paste. The associated Holika Dahan (fire burning) activities will enhance the particle concentration and alter chemistry of the local environment. Higher aerosol loading during the monsoon period at all wavelengths, noticed in the present study, due to paucity of useful data points and prevalence of turbid atmospheric conditions.

Frame (b) shows the seasonal variation in water vapor. The monthly mean values of the water vapor varied from 1.39 to 3.98 cm, representing a minimum value in January (1.39±0.27) and maximum July (3.98±0.23). It is observed that water vapor is smaller during the month of January and February. It starts increasing from March with the onset of the hot summer season and reaches maximum during the months of the southwest monsoon season (June-September). However, the number of days of observations during June-September is less because of a smaller number of clear/partly clear sky days. Therefore, the relative magnitude of water vapor during these four months could be partly due to sampling bias. However, the average value of water vapor during the monsoon season is still significantly higher when compared to other seasons. Water vapor starts decreasing once the monsoon season ends in September. Lower values are observed in winter, slightly increasing up to monsoon season and thereafter water vapor is decreasing due to monsoon rains and decreased aerosol input due to colder ground surface. The less possibility of hygroscopic growth of aerosols due to low water vapor content may also contribute. On a seasonal scale, the increase water vapor from the winter (December-February) to pre-monsoon (March-May) season is about 39.72% and from the pre-monsoon to monsoon (June-September) seasons is as high as 80.95%.

Frame (c) illustrates the mean seasonal variation in Ångstrom Exponent. The Ångström exponent ($\alpha_{440-870}$) is determined from the spectral dependence of the measured optical depth and is a measure of the relative dominance of fine (submicron) aerosols over the coarse (micron-size) aerosols (Kumar et al., 2011) as shown in the Frame (d). Higher values of alpha indicate the dominance of fine particles, whereas lower values indicate the dominance of coarse particles and relatively less concentration of fine particles. It is expected that when the aerosol particles are very small, on the order of air molecules, $\alpha_{440-870}$ should approach 4 and it should approach 0 for very large particles (Holben et al., 2001). The decrease of α from winter to pre-monsoon, and monsoon months is indicative of increased coarse-mode particle contribution, consistent dust particles (>10 μm) in the aerosol loading. This strong decrease in $\alpha_{440-870}$ value could be due to mixing of air

originating from oceanic and desert regions. The notable lower values of the Ångström Exponent during June-September are ascribed to be due to cloud contamination of data retrievals caused by thin invisible cirrus (Chew et al., 2011; Huang et al., 2012).

Figure (e) portrays mean seasonal variation in aerosol size distribution. It is clear from the figure that during monsoon season, coarse-mode volume concentration is higher than the fine-mode which suggests that there is dominance of coarse- mode aerosol particles over the site due to the monsoon activities that start during this season and also due to local meteorological conditions, land-surface and long-range transport processes. Tripathi et al. (2005) found that there was an increase of 50% in volume concentration in coarse mode over the Indian region during the monsoon season. On the other hand, there is a very small variation in mean radius of fine-mode aerosol particles in comparison to coarse-mode during post-monsoon and winter seasons, which suggest that there may be different types of sources of coarse-mode particles. The errors associated with the particle retrieval in the size range ($0.1 \leq r \geq 7$ μm) do not exceed 10% in the maxima of the size distribution and may increase up to about 35% for the points corresponding to the minimum values of dV(r)/dlnr in this size range (Dubovik et al., 2002).

Frame (f) depicts the seasonal dependence of Single Scattering Albedo (SSA) during different seasons. SSA is calculated from the scattering optical thickness which is obtained from the normalized aerosol phase function using diffuse radiance measured at different angles. The detailed method of determining the SSA was given by Dubovik et al. (1998). SSA has nearly a unit value for purely scattering aerosols (e.g. sulphate aerosols) and has low value for strongly absorbing aerosols (e.g. black carbon and/or mineral dust). The mean seasonal variation of SSA at different wavelengths during the study period shows increase in SSA from winter to monsoon due to the dominance of anthropogenic aerosols in the atmosphere. It can also be seen that during post-monsoon and winter, SSA decreases with wavelength due to dominance of absorbing aerosols over the experimental site, which is attributed to presence of a mixture of aerosols from multiple sources like vehicular and industrial pollution, and biomass burning in the field. But in pre-monsoon, SSA values are slightly higher at 1020nm, compared to 440nm. This suggests that the dominance of dust and marine events, thus enhancement in the scattering contribution of coarse particle. The atmosphere contains more water-soluble particles, in conditions like those found by Singh et al. (2004) in Kanpur, India. In addition, for locations closer to the ocean, the air is more humid during summer leading to enhanced water uptake of the water-soluble particles fraction. But monsoon to

post-monsoon, the SSA values are slightly low, which suggests a possible combination of urban industrial particles and sea salt aerosols over the region.

Frame (g) depicts the seasonal dependence of Asymmetry Parameter (AP) during different seasons. Theoretically, the range of AP lies between -1 (for the backward scattered radiation) to +1 (for the forward scattered radiation). However, the zero value represents symmetric scattering. There is relatively little variation in AP among these four seasons at shorter wavelength (440nm), while AP was larger at 440nm in monsoon season compared to other wavelengths (675, 870, and 1020nm). The greater relative contribution of coarse-mode particles to the aerosol size distribution might have resulted in a phase function shift toward greater forward scattering at the longer (infrared) wavelengths and very little change in the shorter (visible) wavelength. The AP is also wavelength dependent and varies from 0.71±0.01 to 0.65±0.04 during the whole period.

Frames (h) and (i) depict the wavelength dependence of real and imaginary parts of Refractive Index (RI), respectively, during different seasons. The refractive index is a complex quantity, expressed in terms of real $n(\lambda)$ and imaginary $k(\lambda)$ parts; which provide an indication of highly scattering or highly absorbing types of aerosols, with higher $n(\lambda)$values corresponding to the scattering type and higher $k(\lambda)$ values corresponding to the absorbing type (Sinyuk et al., 2003). Real and imaginary parts $n(\lambda)$ and $k(\lambda)$, are not independent of SSA and the retrieved size distribution of the aerosols in the region, but some differences in trends may be observed because of the presence of different types of aerosols (Dubovik et al., 2002). The useful information about the RI comes from aureole radiances, which are strongly affected by errors in the angle-pointing bias. The errors are estimated to be 30-50% for the imaginary part and ±0.04 for the real part of the RI (Dubovik et al., 2002). These estimated errors are for high aerosol loading ($AOD_{440nm} \geq 0.5$) at solar zenith angle >50^{o}.

The seasonal variation of real part of RI shows increase in real part of values with increase in wavelength. While $n(\lambda)$ is highest (>1.52) at all wavelengths during the pre-monsoon season in the years 2005–2015, showing the higher scattering optical state of the atmosphere during this period. This is also supported by the higher SSA in the year 2005–2015. However, lower $n(\lambda)$ values during the post-monsoon season could probably be associated with higher relative humidity and resultant hygroscopic growth, similar to the conditions found over Goddard Space Flight Center (Dubovik et al., 2002). During the pre-monsoon season, $n(\lambda)$ values at higher wavelengths are close to the $n(\lambda)$ values of dust (1.53) found from several models (World Meteorological

Organization (WMO), 1983; Koepke et al., 1997), clearly indicating the contribution of dust to the optical properties. However, the $n(\lambda)$ during the monsoon and winter seasons have intermediate values. The lowest value in post-monsoon is due to the anthropogenic activities. The real part of refractive index of dust aerosol is usually greater than that of the anthropogenic aerosols (Alam et al., 2011).

The imaginary value is found to be higher in winter and lower in monsoon, with higher values relating to absorbing anthropogenic aerosols and the lower values to dust aerosols. The imaginary part is highest during December, which shows that anthropogenic aerosols are dominant during this period. The higher imaginary part values at the two shortest wavelengths (440nm and 670nm) are attributed to the absorption of organic carbon/black carbon (Arola et al., 2011). On the contrary, the imaginary part values are lower in monsoon season. This suggests that dust aerosols are dominant during the monsoon season, similar to the conditions found in Kanpur region, India (Singh et al., 2004).

Frames (j) and (k) indicate seasonal variation in Effective Radius (Reff) and volume-weighted mean radius (Rv), respectively. Effective Radius (R_{eff}) is quite representative of the optical properties of coarse-mode particles, whereas for fine particles, volume weighted mean radius (Rv) is more appropriate parameter (Tanré et al., 2001). R_{eff} is found to be higher during the pre-monsoon and monsoon seasons. The high values in R_{eff} during the monsoon season are attributed to the abundant transport of aerosols of natural origin and also the surface-level anthropogenic aerosols, which increases the loading of coarse-mode particles (Vijayakumar et al., 2012). The increase and decrease in R_{eff} during post-monsoon and winter seasons respectively, are interesting. Although no significant coarse-mode particle loading takes place during post-monsoon and the hygroscopic growth of these particles are unlikely, the effective radius of coarse-mode particles may increase if the fine-mode particles get attached to the surface of the coarse-mode particles. However, R_{eff} has not been found to increase significantly, because it is more influenced by the number concentration compared to the volume concentration. The increase in Rv is attributed to the hygroscopic growth of the fine-mode particles. The seasonal variability in coarse-mode particles (R_{eff}) is found to be more as compared to that of fine-mode particles (Rv) with maximum during monsoon season; due to changes in circulation, land-surface and long-range transport processes.

5.9. Long-term trends and changes in aerosol products at different wavelengths

The long-term trends in monthly average values have been calculated from the daily average AODs at 440, 675, 870 and 1020 nm during the study period. Figures 13, 14, 15, 16 depict the long-term trends in monthly average values, calculated from the daily average AOD(a), SSA (b), Asymmetry Parameter (c), RI (real) (d) and RI (imaginary) (e) at 440 nm, 675nm, 870nm and 1020 nm, respectively. It is evident from the frame (a) that the AODs are strongly dependent on receiving filter centre wavelength, resemble that of a continental environment (Vijayakumar et al., 2012) whereas flat spectra are generally expected over marine and dust environments (Kumar and Devara, 2012a). AOD at 440nm shows increasing trend because this region is mainly affected by various kinds of aerosol sources (Vijayakumar et al., 2012) and change of meteorological patterns. The variations in SSA at 440nm (frame b) reveals the influence of dust and urban pollution, with the SSA tending to increase rapidly with wavelength during dust events but to decrease during periods of increased urban pollution (Bergstrom et al., 2007; Dubovik et al., 2002). The percentage increase in trend and other statistical parameters are provided in a table to follow. The increase in SSA with wavelength suggests an enhanced mixed aerosols and biomass-generated aerosols along with urban-industrial aerosols (Bergstrom et al., 2007; Russel et al., 2010). Thus, the results clearly suggest the spectral behavior of SSA highly depends on the nature of aerosol particles. It can be seen from the frame (c) of variations in asymmetry parameter (AP) at 440nm indicates the dependency of AP on aerosol particle size and composition. The AP decrease with increase in wavelength and the overall range varies from 0.71 to 0.65 for the four wavelengths. Zege et al. (1991) showed that the asymmetry parameter ranges from ~0.1 to ~0.75 for very clean atmospheres to heavily polluted conditions. The time series plot of monthly average values of asymmetry parameter over this region shows increasing trend by 0.06% per year at 440nm. The variations in refractive index (both real and imaginary) are shown in frames d and e, respectively. The real part of RI at higher wavelengths is larger than at shorter wavelengths (as shown in the figures to follow) due to the higher absorption at longer wavelengths by coarse particles (Cheng et al., 2006a, 2006b).

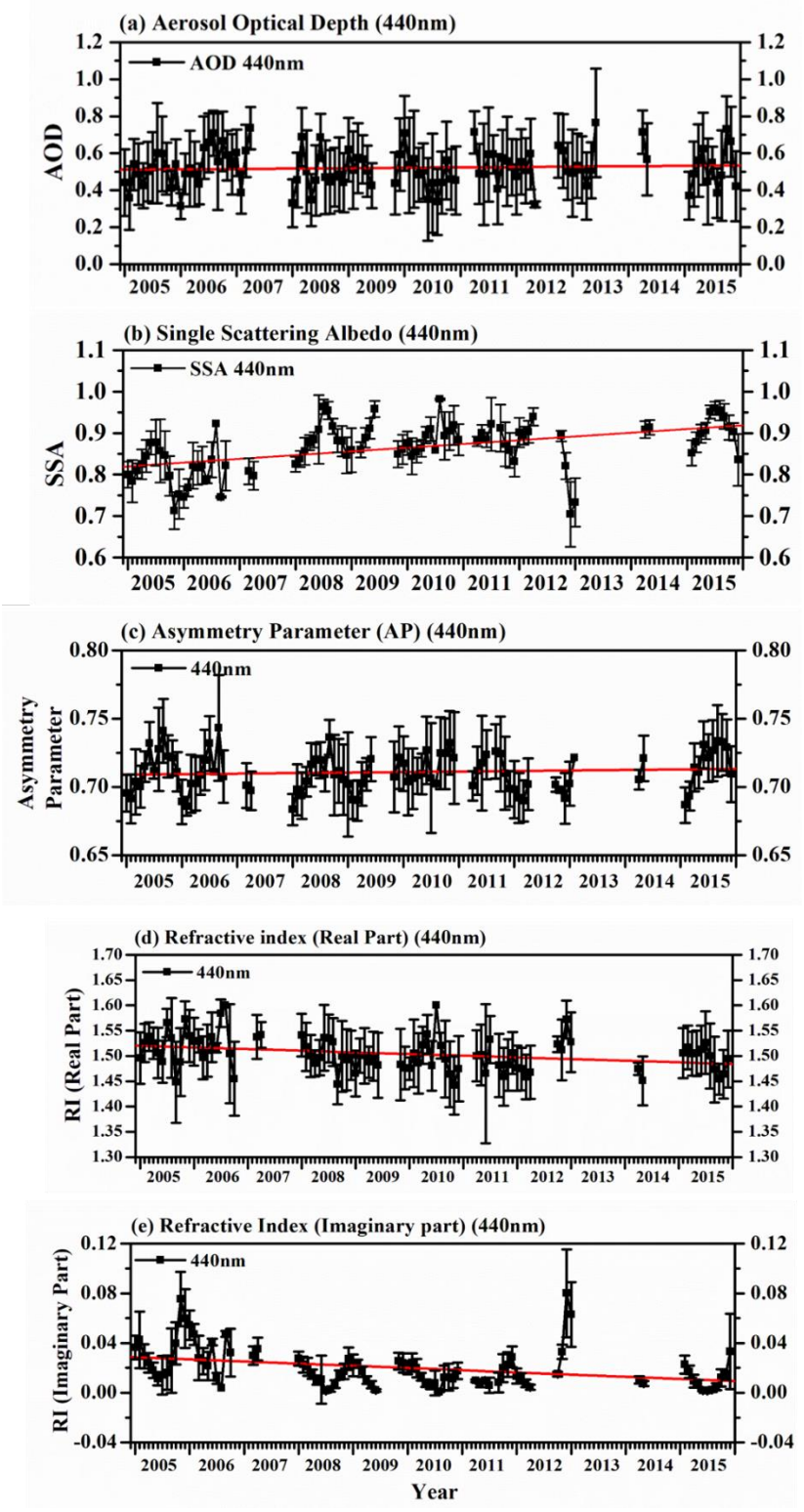

Figure 13: Long-term trends in aerosol products at 440 nm.

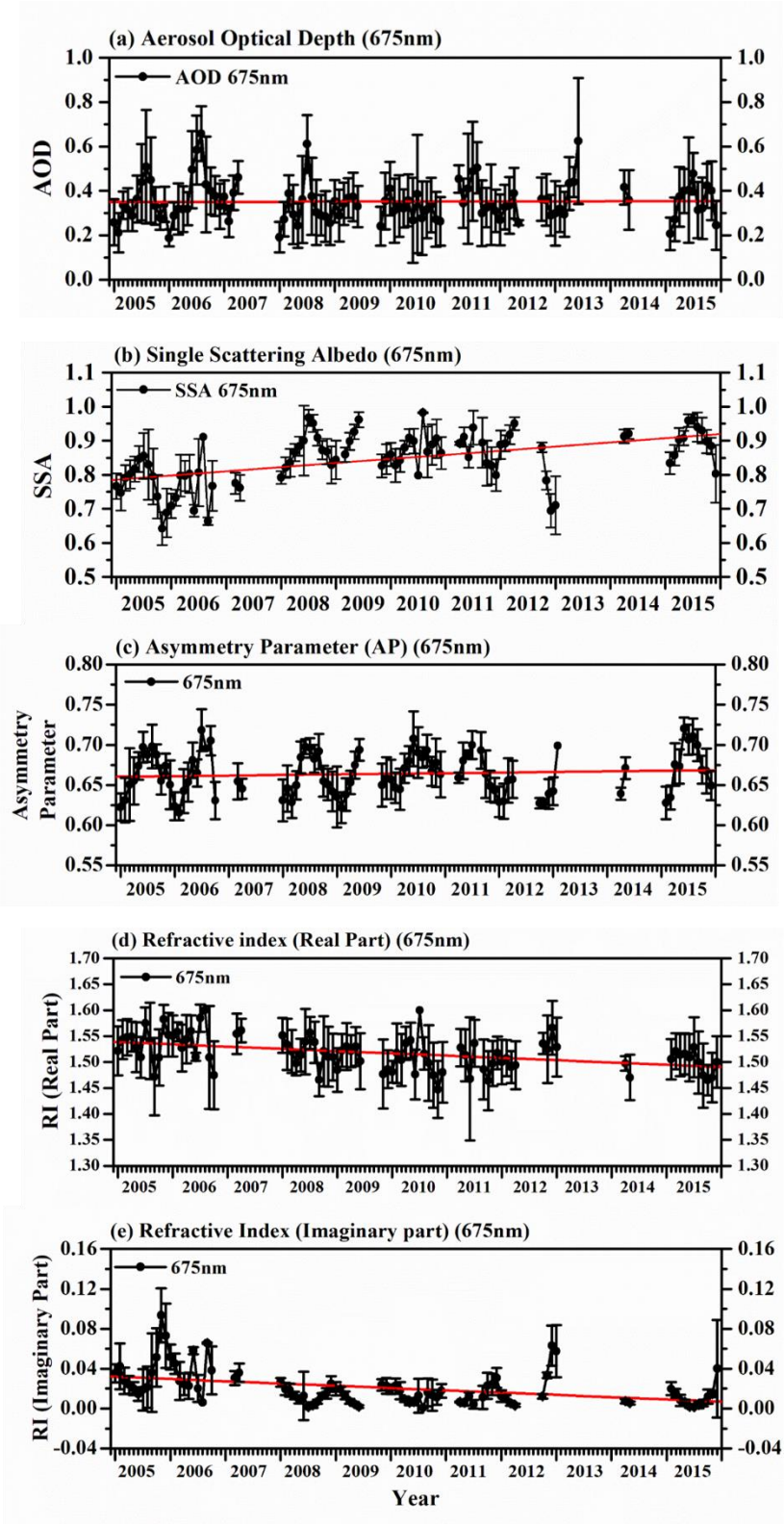

665 **Figure 14**: Same as Fig. 13, but for 675 nm.

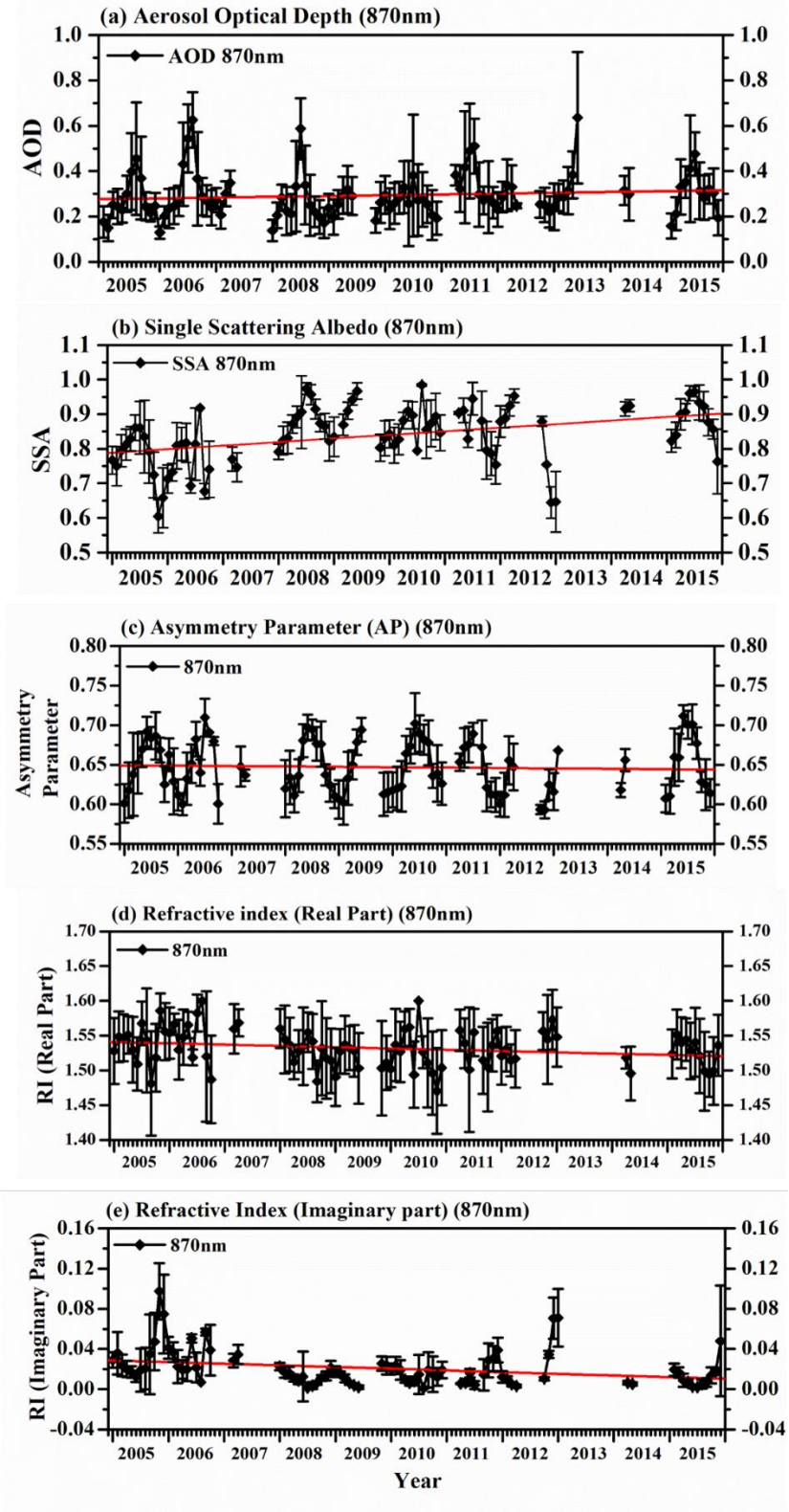

Figure 15: Same as Fig. 13, but for 870 nm.

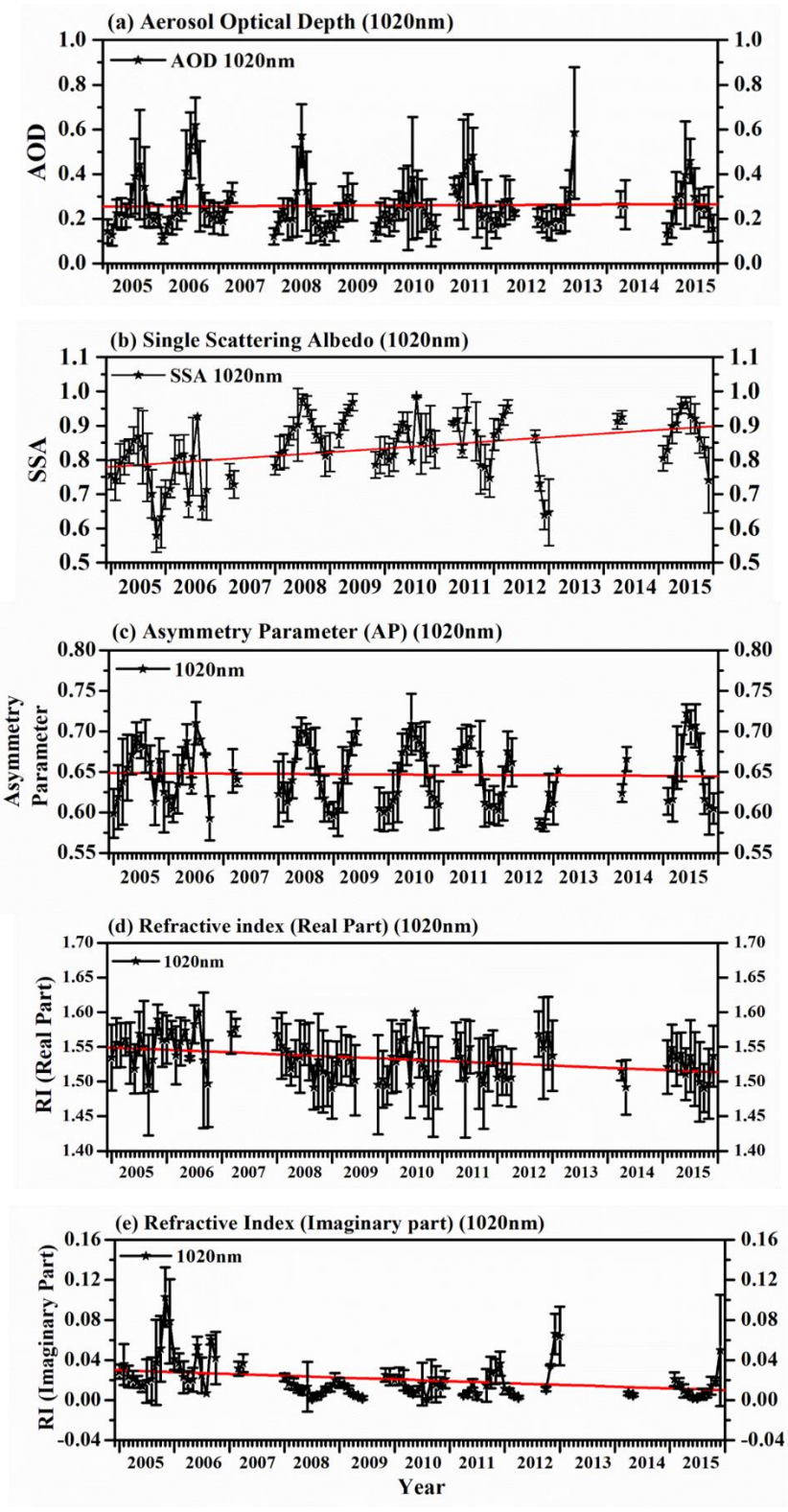

670 **Figure 16**: Same as Fig. 13, but for 1020 nm.

Average values, calculated from the daily average AOD (a), SSA (b), Asymmetry Parameter (c), RI (real) (d) and RI (imaginary) (e) at 675 nm are shown in Fig. 14. Similarly, the long-term trends and changes in the above aerosol products, AOD (a), SSA (b), AP (c), RI (real) (d) and RI (imaginary) (e) at 870 and 1020 nm are plotted in Figures 15 and 16. Considering the above, long-term trends in aerosol products, considered in the study, depend mainly on source characteristics, size distribution and phase. Information on the statistical parameters is tabulated in Table 3.

Table 3. Statistical information on the trend analysis of different aerosol products.

S. No.	Parameter	Wavelength (nm)	Fitting line	R	SD	No. of points	Trend (Per year)
1	Aerosol Optical Depth (AOD)	440nm	Y=1.80E-4X+0.51	0.07	0.10	96	0.50%
		675nm	Y=2.77E-5X+0.35	0.01	0.09	96	0.09%
		870nm	Y=2.95E-4X+0.27	0.11	0.09	96	1.56%
		1020nm	Y=8.20E-5X+0.25	0.03	0.10	96	0.47%
2	Single Scattering Albedo (SSA)	440nm	Y=7.54E-4X+0.82	0.47	0.05	84	1.34%
		675nm	Y=0.001X+0.78	0.49	0.07	84	1.86%
		870nm	Y=8.61E-4X+0.79	0.38	0.08	84	1.56%
		1020nm	Y=8.95E-4X+0.78	0.37	0.08	84	1.60%
3	Asymmetry Parameter (AP)	440nm	Y=3.21E-5X+0.71	0.09	0.01	86	0.06%
		675nm	Y=6.22E-5X+0.65	0.09	0.03	86	0.13%
		870nm	Y=-3.94E-5X+0.65	-0.05	0.03	86	-0.07%
		1020nm	Y=-3.00E-5X+0.65	-0.03	0.04	86	-0.07%
4	Refractive Index (Real Part)	440nm	Y=-2.74E-4X+1.52	-0.31	0.03	85	-0.26%
		675nm	Y=-3.66E-4X+1.54	-0.43	0.03	85	-0.34%
		870nm	Y=-1.53E-4X+1.54	-0.22	0.03	85	-0.14%
		1020nm	Y=-2.69E-4X+1.55	-0.37	0.03	85	-0.25%
5	Refractive Index (Imaginary Part)	440nm	Y=-1.46E-4X+0.02	-0.35	0.02	85	-6.63%
		675nm	Y=-1.89E-4X+0.03	-0.41	0.02	85	-7.73%
		870nm	Y=-1.37E-4X+0.03	-0.29	0.02	85	-6.46%
		1020nm	Y=-1.51E-4X+0.02	-0.32	0.02	85	-6.83%

5.10 Long-term variations in aerosol radiative forcing

685 The monthly average ARF variations at the TOA, BOA (surface) and within the ATM during the study period are plotted in Figure 17. The decreasing trend of radiative forcing in the ATM and at TOA reveals dominance of hygroscopic (scattering) particles whereas the increasing trend of radiative forcing at BOA indicate the dominance of hydrophobic (absorbing) aerosol particles.

The BOA forcing is found to be negative, while ATM is positive for all months These interactions between aerosols and solar radiation can be attributed to combination of aerosol properties (i.e. types), surface properties (i.e. albedo) and geographical parameters (latitude, season) (Yu et al., 2006). The large difference between TOA and BOA forcing demonstrate that solar radiation is being absorbed within the atmosphere, and as a result the atmosphere gets warmer, but the earth's surface gets cooler (Alam et al., 2011; Kumar and Devara, 2012b). This can substantially alter the atmospheric stability and influence the dynamic system of the atmosphere (Li et al., 2010). The ARF during winter, the BOA is more strongly negative associated with the corresponding TOA, giving rise to the highest ATM. As against this, during pre-monsoon and post-monsoon seasons, ATM appears to be reduced with reduced heating rate. The monthly average ARF variations at the TOA, BOA (surface), and within the ATM (atmosphere) during the study period are shown in Fig. 26. The decreasing trend of radiative forcing in the ATM and at TOA reveals dominance of hygroscopic (scattering) particles whereas the increasing trend of radiative forcing at BOA indicate the dominance of hydrophobic (absorbing) aerosol particles. The BOA forcing is found to be negative, while ATM is positive, for all months. ATM forcing will increase if aerosol forcing at the TOA is more toward positive side while there is a large negative forcing at surface level. But TOA shows almost minor variation between positive and negative. Seasonal variations of radiative forcing at TOA, BOA and ATM are shown in Table 1. It shows very high atmospheric heating (more than 60 Wm^{-2}) at the all seasons. These interactions between aerosols and solar radiation can be attributed to combination of aerosol properties (i.e., types), surface properties (i.e., albedo), and geographical parameters (latitude, season) (Yu et al., 2006). The large difference between TOA and BOA forcing demonstrate that solar radiation is being absorbed within the atmosphere, and as result the atmosphere gets warmer but the earth`s surface gets cooler (Alam et al., 2011; Kumar and Devara, 2012b). This can substantially alter atmospheric stability and influence the dynamic system of the atmosphere (Li et al., 2010). The ARF for the whole observation period at the TOA is in the range of +11 to -46 Wm^{-2} (average -17±10 Wm^{-2}), at the BOA from -32 to -152 Wm^{-2} (average -82±19 Wm^{-2}), increasing the ATM forcing from +15 to +149 Wm^{-2} (average +64±25 Wm^{-2}). But the radiative forcing during winter, the BOA (–73.3±18.2 Wm^{-2}) is more strongly negative associated with corresponding TOA (–14.8±9.5 Wm^{-2}), giving rise to the highest ATM value of 58.4±15.5 Wm^{-2} with a resulting heating rate of 1.95±0.5 $Kday^{-1}$ during this season.

As against this, during pre-monsoon and post-monsoon seasons, ATM appears to be reduced with the reduced heating rates of 1.7±0.5 Kday^{-1} and 1.8±0.5 Kday^{-1}.

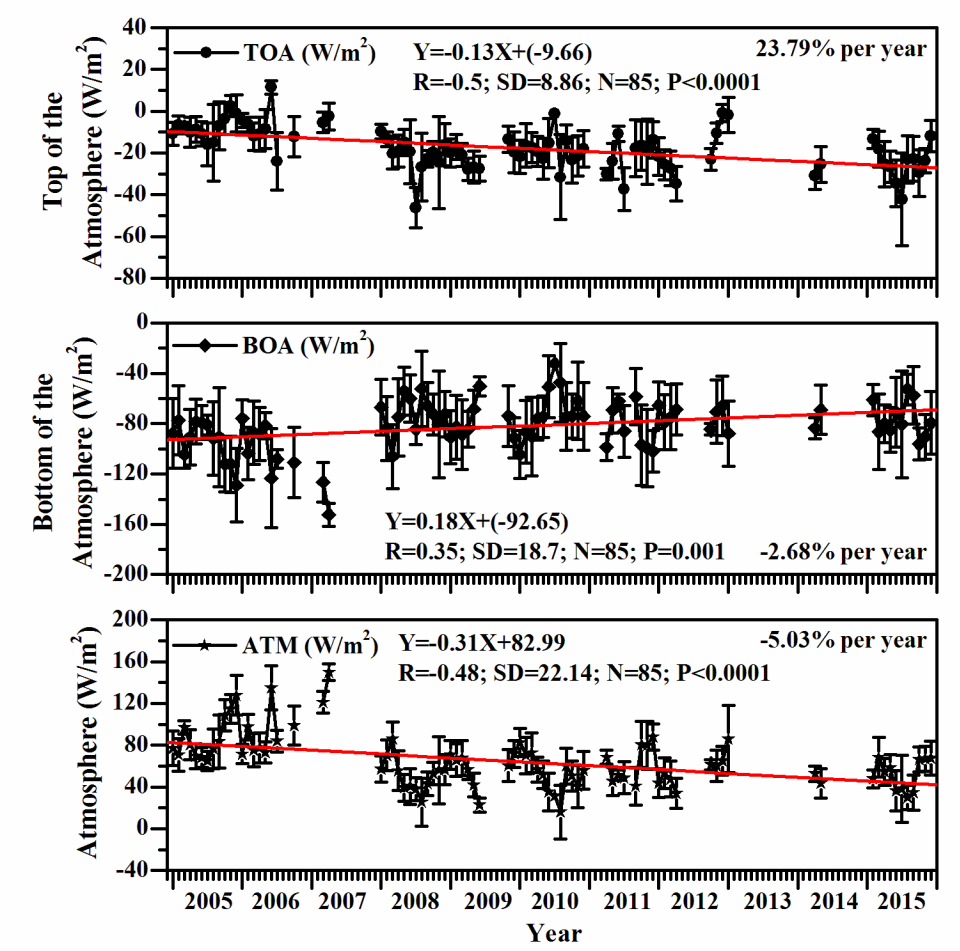

Figure 17. Long-term monthly mean variation in radiative forcing at Top of the Atmosphere (TOA; Wm^{-2}), Bottom of the Atmosphere (BOA; Wm^{-2}), and in the Atmosphere (ATM; Wm^{-2}). Vertical bar at each data point represents standard deviation from mean.

5.11 Comparison between AERONET observations with satellite observations

Figure 18 depicts the comparison between long-term climatology of AOD and Water vapor data sets from AERONET observations with MODIS and OMI observations. Here MODIS satellite gives AOD at 550nm, while AERONET data had no corresponding wavelength to match it exactly. So, the AERONET AOD at 550 nm was obtained by interpolation between 440 nm and 675 nm following the Ångström equation. All figures clearly show increasing trend except water vapor parameter. Figure 18(b) clearly shows, AERONET AOD observations were relatively higher over-

estimation compared to OMI AOD. The possible reasons for relatively less correlation observed between the AODs recorded by AERONET and OMI have been explained. Frame (c) shows AERONET H_2O trend is higher compared to satellite H_2O trend, but magnitude wise both are following similar trend. Figure 19 shows correlation between AERONET observations and satellite observations. They show strong correlation between satellite observations and AERONET data (Figures 19(a), and (c)). Weak correlation (Figure 19(b)) was observed between OMI AOD_{442nm} and AERONET AOD_{440nm}. Apart from a small sensing wavelength difference of 2 nm, higher AOD values by AERONET and relatively lower values by OMI have also been reported by Humera et al. (2015) due to anthropogenic activity and biomass burning. Now the correlation has been improved by reducing the scatter (eliminating the significant out-layered data points) between the observations.

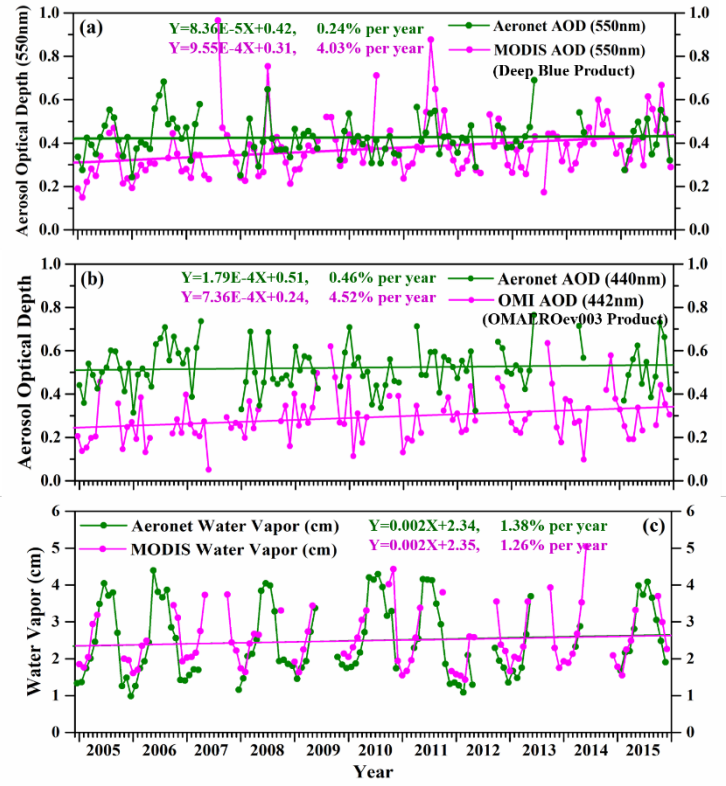

Figure 18. Long-term monthly mean variation of AOD, and Water vapor (cm) data sets from ground-based and satellite observations.

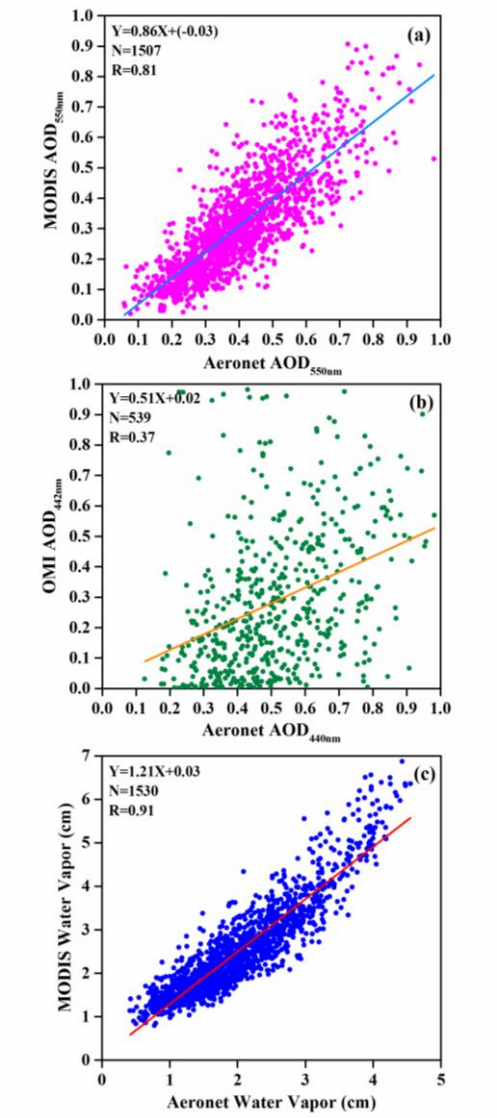

Figure 19. Correlation between (a) Aeronet AOD at 550nm with MODIS AOD at 550nm, (b) Aeronet AOD at 440nm with OMI AOD at 442nm, and (c) Aeronet water vapor (cm) with MODIS water vapor (cm).

6 Conclusions

Long-term detection of changes in aerosol characteristics has been one of the key issues for researchers working on climate and environment. AERONET, the largest global network for ground-based remote sensing of aerosol optical properties, has grown rapidly, and more than ten years of continuous observations have been maintained by a large number of independent academic and research institutions. The high quality and accuracy of AERONET observations

provided a tremendous opportunity to investigate how and what causes the changes in AOD (Wu and Zeng, 2011). The main conclusions that can be drawn from the present study are summarized as follows:

1. Time series of AOD exhibit an increasing trend over Pune during the study period (January 2005 - December 2015), which is ascribed mainly to growth in urbanization. The daily variability of AOD was found to be higher in monsoon and lower in winter months, corresponding to the changes in season. The relative increase of aerosol loading during the monsoon season is considered to be due to dominance of aerosols of marine origin at the study region.
2. The long-term variations in columnar water vapor also showed increasing trend at a rate of $1.16\%Yr^{-1}$, which is found responsible for the increasing trend in AOD, particularly during monsoon season.
3. The Ångström Exponent showed decreasing trend from January 2005 to December 2015, exhibiting seasonal dependence. The relationship between AE and AOD suggests that experimental region is characterized by different types of aerosols and their transport by regional air mass changes from season to season.
4. The increase in fine-mode fraction of composite aerosol is found to be marginal as compared to that of coarse-mode, which reveals dominance of natural processes against anthropogenic sourcesat the study location.
5. The seasonal variability in coarse-mode particles (R_{eff}) is found to be more as compared to that of fine-mode particles (R_v) with maximum during monsoon season due to changes in circulation, land surface and long-range transport and the relatively higher contribution of the coarse-mode particles to the observed AOD as compared to that of fine-mode particles.
6. Long-term climatology of SSA shows increasing trend. It is 1.34% per year at 440, 1.86% per year at 675, 1.56% per year at 870 and 1.60% per year at 1020nm. Furthermore, the spectral mean SSA values for all wavelengths show decrease with increasing wavelength, which suggests an enhanced mixed aerosols and biomass burning generated aerosols along with urban-industrial aerosols.
7. The decrease in ASP values from monsoon to post-monsoon and winter due to transport of dust is gradually decreased and a significant fraction of total aerosol load in this region consists of fine anthropogenic particles.

8. The aerosol radiative forcing (ARF) for the whole observation period at the top of the atmosphere (TOA) is in the range of +28 to -60 Wm^{-2} (average -17±12 Wm^{-2}), at the bottom of the atmosphere (BOA) from -48 to -233 Wm^{-2} (average -86±30 Wm^{-2}), increasing the atmosphere (ATM) forcing from +16 to +210 Wm^{-2} (average +68±34 Wm^{-2}).
9. Aerosol types showed dominance of mixed type of aerosols (44.85%) followed by biomass burning and urban industrial aerosols (22.57%).
10. The AERONET data provides high quality and accuracy, as compared to satellite remote sensing data, though the spatial coverage of AERONET is relatively limited. However, the ground-based networks have been widely used to validate and help interpreting the results from satellite sensors and model simulations.

Code/Data Availability. The work reported in this manuscript is a part of the joint collaborative research program between Amity University Haryana (AUH), Manesar-Gurgaon, India; Sri Venkateswara University, Tirupati, India; Indian Institute of Tropical Meteorology, Pune, India; Science Systems and Applications (SSA), Inc., Lanham, MD 20706, USA; and NASA Goddard Space Flight Center (GSFC), Greenbelt, MD 20771, USA. However, maximum part of the data has already been made available in our published papers as detailed below:

Kumar, S., Devara, P. C. S., Dani, K. K., Sonbawne, S. M., Saha, S. K.: Sun-Sky Radiometer–Derived Column-Integrated Aerosol Optical and Physical Properties over a Tropical Urban Station during 2004–2009, Journal of Geophysical Research: Atmospheres,116: D10201, doi: 10.1029/2010JD014944, 2011.

P. Khatri, T. Takamura, T. Nakajima, V. Estellés, H. Irie, H. Kuze, M. Campanelli, A. Sinyuk, S. -M. Lee, B. J. Sohn, G. Padhithurai, S. -W. Kim, S. C. Yoon, J. A. M. Lozano, M. Hashimoto, P. C. S. Devara, and N. Manago (2016): Factors for inconsistent aerosol single scattering albedo between SKYNET and AERONET, Journal of Geophysical Research: Atmospheres, 121, 1859-1877.

Author Contribution. All authors have, directly or indirectly, participated in the installation of the sun-sky radiometer, calibration, maintenance, data archival and analysis, attribution of results and manuscript preparation and communication.

Competing Interests. The authors declare that they have no conflict of interest.

Acknowledgements. This work was carried out under a collaboration project between NASA, USA, Indian Institute of Tropical Meteorology (IITM), Pune; Amity University Haryana (AUH), Gurugram and Sri Venkateswara University (SVU), Tirupati, India. The corresponding author (PCSD) express his sincere gratitude to Hon'ble Founder President and Chancellor, and all other authorities of AUH for continuous support, and appreciates his team for cooperation. The principal author (KV) acknowledges the support, in the form of Research Associate (RA) Fellowship, from the Council of Scientific and Industrial Research (CSIR), Government of India, New Delhi. Thanks are due to the Director of IITM, Pune, for the infra-structure facilities. The authors would also like to thank AERONET, NASA, staff for support (http://aeronet.gsfc.nasa.gov/) in calibrating the instrument and processing of the data. We also acknowledge the ECMWF for synoptic meteorological data used in the study. The authors would also like to thank the MODIS, OMI Science teams for providing access to the excellent data products that made this study more effective. The valuable suggestions/remarks of anonymous reviewers are gratefully acknowledged, and they helped to improve the scientific quality and clarity of the study.

References

Abdou, W. A., Diner, D. J., Martonchik, J. V., Bruegge, C. J., Kahn, R.A., Gaitley, B. J., Crean, K. A., Remer, L. A., and Holben, B. N.: Comparison of coincident multi angle imaging spectroradiometer and moderate resolution imaging spectroradiometer aerosol optical depths over land and ocean scenes containing AErosol RObotic NETwork sites, J. Geophys. Res.,110, D10S07, doi:10.1029/2004JD004693, 2005.

Alam, K., Trautmann, T., and Blaschke, T.: Aerosol optical properties and radiative forcing over mega-city Karachi, Atmos. Res., 101, 773–782, 2011.

Alexandrov, M. D., Schmid, B., Turner, D. D., Cairns, B., Oinas, V., Lacis, A. A., Gutman, S. I., Westwater, Ed. R., Smirnov, A., and Eilers, J.: Columnar water vapor retrievals from multi-filter rotating shadow-band radiometer data, J. Geophys. Res., 114, D02306, doi:10.1029/2008JD010543, 2009.

Arola, A., Schuster, G., Myhre, G., Kazadzis, S., Dey, S., and Tripathi, S.N.: Inferring absorbing organic carbon content from AERONET data, Atmos. Chem. Phys., 11, 215–225, 2011.

Aruna, K., Lakshmi Kumar, T. V., Krishna Murthy, B. V., Suresh Babu, S., Venkat Ratnam, M., and Narayana Rao, D.: Short wave Aerosol Radiative Forcing estimates over a semi urban coastal environment in south-east India and validation with surface flux measurements, Atmos. Environ., 125, 418–428, 2016.

Babu, S. S., Satheesh, S. K., and Moorthy, K. K.: Aerosol radiative forcing due to enhanced black carbon at an urban site in India, Geophys. Res. Lett. 29, 1880, http://dx.doi.org/10.1029/2002GL015826, 2002.

Babu, S. S., Moorthy, K. K., and Satheesh, S. K.: Temporal heterogeneity in aerosol characteristics and the resulting radiative impacts at a tropical coastal station. Part 2: direct short wave radiative forcing, Ann. Geophys., 25, 2309–2320, 2007.

Bergstrom, R. W., Pilewskie, P., Russell, P. B., Redemann, J., Bond, T. C., Quinn, P. K., and Sierau, B.: Spectral absorption properties of atmospheric aerosols, Atmos. Chem. Phys., 7, 5937–5943, 2007.

Charlson, R. J., Schwartz, S. E., Hales, R. D., Cess, J. A., Coakley, Jr., Hansen, J. E., and Hofman, D. J.: Climate forcing by anthropogenic aerosols, Science 255, 423–430, 1992.

Cheng, T., Wang, H., Xu, Y., Li, H., and Tian, L.: Climatology of aerosol optical properties in northern China, Atmos. Environ., 40, 1495–1509, 2006a.

Cheng, T., Liu, Y., Lu, D., Xu, Y., and Li, H.: Aerosol properties and radiative forcing in Hunshan Dake desert, northern China, Atmos. Environ., 40, 2169–2179, 2006b.

Chew, B. N., Campbell, J. R., Reid, J. S., Giles, D. M., Welton, E. J., Salinas, S. V., and Liew, S. C.: Tropical cirrus cloud contamination in sun photometer data, Atmos. Environ., 45, 6724–6731,http://dx.doi.org/10.1016/atmosenv.2011.08.017, 2011.

Crutzen, P. J., and Andreae, M. O.: Biomass burning in tropics: impact on atmospheric chemistry and biogeochemical cycles, Science, 250, 1669–1678, 1990.

Devara, P. C. S., Raj, P. E., Sharma, S., and Pandithurai, G.: Long-term variations in lidar-observed urban aerosol characteristics and their connection with meteorological parameters, Int. J. Clim.,14,581–591, 1994.

Devara, P. C. S., Saha, S. K., Ernest Raj, P., Sonbawne, S. M., Dani, K. K., Tiwari, K., and Maheskumar, R. S.: A four-year climatology of total column tropical urban aerosol, ozone and water vapor distributions over Pune, India, Aerosol Air Qual. Res., 5(1), 103–114, 2005.

Devara, P. C. S., Maheskumar, R. S., Raj, P. E., Dani, K. K., and Sonbawne, S. M.: Some features of aerosol optical depth, ozone and Precipitable water content observed over land during the INDOEX-IFP 99, Meteorologische Zeitschrift,10, 123–130, 2001.

Devara, P. C. S., Maheskumar, R. S., Raj, P. E., Pandithurai, G., and Dani, K. K.: Recent trends in aerosol climatology and air pollution as inferred from multi-year Lidar observations over a tropical urban station, Int. J. Clim., 22, 435–449, 2002.

Dubovik, O., Holben, B. N., Kaufman, Y. J., Yamasoe, M., Smirnov, A., Tanré, D., and Slutsker, I.: Single-scattering albedo of smoke retrieved from the sky radiance and solar transmittance measured from ground, J. Geophys. Res., 103, 31903–31924, 1998.

Dubovik, O., Holben, B. N., Eck, T., Smirnov, A., Kaufman, Y. J., King, M., Tanré, D., and Slutsker, I.: 2002. Variability of absorption and optical properties of key aerosol types observed in worldwide locations, J. Atmos. Sci., 59, 590–608, 2002.

Diner, D. J., Asner, G. P., Davies, R., Knyazikhin, Y., Muller, J. -P., Nolin, A. W., Pinty, B., Schaaf, C.B., and Stroeve, J.: New directions in Earth observing: Scientific applications of multiangle remote sensing, Bull. Amer. Meteoro. Soc., 80, 2209–2228, doi:10.1175/1520-0477(1999)0802.0.CO;2, 1999.

Eck, T. F., Holben, B. N., Reid, J. S., Dubovik, O., Smirnov, A., O'Neill, N. T., Slutsker, I., and Kinne, S.: Wavelength dependence of the optical depth of biomass burning, urban, and desert dust aerosols, J. Geophys. Res., 104, 31333–31349, doi:10.1029/1999JD900923, 1999.

Eck, T. F., Holben, B. N., Dubovik, O.,Smirnov, A., Slutsker, I., Lobert, J. M., and Ramanathan, V.: Column-integrated aerosol optical properties over the Maldives during the northeast monsoon for 1998–2000, J. Geophys. Res., 106(28), 555–566, 2001.

Ganguly, D., Jayaraman, A., and Gadhavi, H.: Physical and optical properties of aerosols over an urban location in western India: seasonal variabilities, J. Geophys. Res., 111, D24206, http://dx.doi.rg/10.1029/2006JD007392, 2006.

Garcia, O. E., Diaz, A. M., Exposito, F. J, Diaz, J. P., Dobovik, O., Dubuisson, P., Roger, J. -C., Eck, T. F., Sinuk, A., Derimian, Y., Dutton, E. G., Schafer, J. S., Holben, B. N., and Garcia, C.A.: Validation of AERONET estimates of atmospheric solar fluxes and aerosol radiative

forcing by ground-based broadband measurements, J. Geophys. Res., 113(D21), https://doi.org/10.1029/2008JD010211, 2008.

Garcia, O., Diaz, J., Exposito, F., Diaz, A., Dubovik, O., Dubuisson, P., and Roger, J. C.: Short wave radiative forcing and efficiency of key aerosol types using AERONET data, Atmos. Chem. Phys., 12, 5129–5145, 2012.

Giles, D. M., Holben, B. N., Tripathi, S. N., Eck, T. F., Newcomb, W. W., Slutsker, I., Dickerson, R. R., Thompson, A. M., Mattoo, S., Wang, S. H., Singh, R. P., Sinyuk, A., and Schafer, J. S.: Aerosol properties over the Indo-Gangetic plain: a mesoscale perspective from the TIGERZ experiment, J. Geophys. Res., 116, http://dx.doi.org/ 10.1029/2011JD015809, 2011.

Giles, D. M., Holben, B. N., Eck, T. F., Sinyuk, A., Smirnov, A., Slutsker, I., Dickerson, R. R., and Thompson, A. M., Schafer, J. S.: An analysis of AERONET aerosol absorption properties and classifications representative of aerosol source regions, J. Geophys. Res. Atmos., 117, D17203, https://doi.org/10.1029/2012JD018127, 2012.

Giles, D. M., Sinyuk, A., Sorokin, M. G., Schafer, J. S., Smirnov, A., Slutsker, I., Eck, T. F., Holben, B. N., Lewis, J. R., Campbell, J. R., Welton, E. J., Korkin, S.V., and Lyapustin, A. I.: Advancements in the Aerosol Robotic Network (AERONET) Version 3 database – automated near-real-time quality control algorithm with improved cloud screening for Sun photometer aerosol optical depth (AOD) measurements, Atmos. Meas. Tech. 12, 169–209, http://doi.org/10.5194/amt-12-169-2019, 2019.

Gobbi, G. P., Kaufman, Y. J., Koren, I., and Eck, T. F.: Classification of aerosol properties derived from AERONET direct sun data, Atmos. Chem. Phys., 7, 453-458, https://doi.org/10.5194/acp-7-453-2007, 2007.

Hansen, J., Sato, M., Ruedy, R., Lacis, A., and Oinas, V.: Global warming in the twenty-first century: An alternative scenario, Proc. Natl. Acad. Sci. U. S. A., 97, 9875–9880, 2000.

He, Z. Z., Mao, J. K., and Han, X. S.: Non-parametric estimation of particle size distribution from spectral extinction data with PCA approach, Powder Technol., 325, 510–518, 2018.

Holben, B. N., Eck, T. F., Slutsker, I., Tanre, D., Buis, J. P., Setzer, A., Vermote, E., Ragan, J. A., Kaufman, Y. J., Nakajima, T., Lavenu, F., Jankowiak, I., and Smirnov, A.:AERONET–A federated instrument network and data archive for aerosol characterization, Remote Sens. Environ., 66, 1–16, doi:10.1016/S0034-4257(98)00031-5, 1998.

Holben, B. N.,Tanré, D., Smirnov, A., Eck, T. F., Slutsker, I., Abuhassan, N., Newcomb, W. W., Schafer, J. S., Chatenet, B., Lavenu, F., Kaufman, Y. J., Vande Castle, J., Setzer, A., Markham, B., Clark, D., Frouin, R., Halthore, R., Karneli, A., O`Neill, N. T., Pietras, C., Pinker, R. T., Voss, K., and Zibordi, G.:An emerging ground–based aerosol climatology: Aerosol optical depth from AERONET, J. Geophys. Res., 106(D11), 12067–12097, doi:10.1029/2001JD900014, 2001.

Hoppel, W.A., Fitzgerald, J.W., and Larson, R.E.: Aerosol size distributions in air masses advecting off the east coast of the United States, J. Geophys. Res., 90, 2365–2379, 1985.

Hsu, N. C., Hermann, J. R., and Weaver, C.: Determination of radiative forcing of Saharan dust using combined TOMS and ERBE data, J. Geophys. Res., 108, 20649–20661, 2000.

Huang, J. F., Hsu, N. C., Tsay, S. C, Holben, B. N., Welton, E. J., Smirnov, A., Hansell, R. A., Berkoff, T. A., Liu, Z. Y., Liu, G. R., Cambell, I. R., Liew, S. C., Jeong, M. J., and Bames, I. E.: Evaluations of cirrus contamination and screening in ground aerosol observations using collocated lidar systems, J. Geophys. Res.-Atmos., 117, D15204, 2012.

Humera, B., Khan, A., Farrukh, C., Samina, B., Imran, S., and Thomas, B.: Inter-comparison of MODIS, MISR, OMI and CALIPSO aerosol optical depth retrievals for four locations on the Indo-Gangetic plains and validation against AERONET data, Atmos. Environ., 111, 113–126, 2015.S

IPCC (Intergovernmental Panel on Climate Change).: Climate Change 2001: The scientific basis-contribution of Working Group I to the third assessment report of the Intergovernmental Panel on Climate Change, Cambridge Univ. Press, New York, 2001.

IPCC (Intergovernmental Panel on Climate Change).: Climate Change 2007: The scientific basis-contribution of Working Group I to the fourth assessment report of the Intergovernmental Panel on Climate Change, Cambridge Univ. Press, New York, 2007.

Kacenelenbogen, M., Leon, J-F., Chiapello, I., and Tanré, D.: Characterization of aerosol pollution events in France using ground-based and POLDER-2 satellite data, Atmos. Chem. Phys., 6, 4851–4866, 2006.

Kaskaoutis, D. G., Badarinath, K. V. S., Kharol, S. K., Sharma, A. R., and Kambezidis, H. D.: Variations in the aerosol optical properties and types over the tropical urban site of Hyderabad, India, J. Geophys. Res.,114, D22204, doi: 10.1029/2009JD012423, 2009.

Kaskaoutis, D. G., Sinha, P. R., Vinoj, V., Kosmopoulos, P. G., Tripathi, S. N., Misra, A., Sharma, M., and Singh, R. P.: Aerosol properties and radiative forcing over Kanpur during severe aerosol loading conditions, Atmos. Environ.,79, 7–19, 2013.

King, M. D., Kaufman, Y. J., Tanré, D., and Nakajima, T.: Remote sensing of tropospheric aerosols from space: past, present, and future, Bull. Amer. Meteor. Soc., 80, 2229–2259, 1999.

Koepke, P., Hess, M., Schult, I., and Shettle, E. P.: Global aerosol data set, MPI Meteorol. Hamb. Rep, pp., 243, 44, 1997.

Kumar, S., Devara, P. C. S., Dani, K. K., Sonbawne, S. M., and Saha, S. K.: Sun-sky radiometer–derived column-integrated aerosol optical and physical properties over a tropical urban station during 2004–2009, J. Geophys. Res.,116, D10201, doi: 10.1029/2010JD014944, 2011.

Kumar, S., and Devara, P. C. S.: Aerosol characterization: comparison between measured and modelled surface radiative forcing over Bay of Bengal, Rem. Sens. Lett., 3(5), 373–381, doi:10.1080/01431161.2011.600466, 2012a.

Kumar, S., and Devara, P. C. S.: A long-term study of aerosol modulation of atmospheric and surface solar heating over Pune, India, Tellus B64, 18420, doi:http://dx.doi.org/10.3402/tellusb.v64i0.18420, 2012b.

Kumar, K. R., Sivakumar, V., Reddy, R. R., Gopal, K. R., and Adesina, A. J.: Inferring wavelength dependence of AOD and Ångström exponent over a sub-tropical station in South Africa using AERONET data: Influence of meteorology, long-range transport and curvature effect, Sci. Total Environ., 461, 397–408, 2013.

Kumar, K. R., Kang, N., and Yin, Y.: Classification of key aerosol types and their frequency distributions based on satellite remote sensing data at an industrially polluted city in the Yangtze River Delta, China, Int. J. Clim., 38, 320–336, 2018.

Lee, J., Kim, J., Song, C. H., Chun, Y., Sohn, B. J., and Holben, B. N.: Characteristics of aerosol types from AERONET sunphotometer measurements, Atmos. Environ., 44, 3110–3117, 2010.

Li, Z., Lee, K. -H., Wang, Y., Xin, J., Hao, and W. -M.: First observation-based estimates of cloud-free aerosol radiative forcing across China, J. Geophys. Res. Atmos., 115(D00K18), 2010.

Liou, K. N.: An Introduction to Atmospheric Radiation, Academic press, 2002.

Mishchenko, M. I., Geogdzhaye, I. V., Rossow, W. B., Cairns, B., Carlson, B. E., Lacis, A. A., Liu, L., and Travis, L. D.: Long-term satellite record reveals likely recent aerosol trend,Science,315,1543, doi:10.1126/science.1136709, 2007a.

Mishchenko, M. I., Cairns, B., Hansen, J. E., Travis, L. D., Kopp, G., Schueler, C. F., Fafaul, B. A., Hooker, R. J., Maring, H. B., and Itchkawich, T.: Accurate monitoring of terrestrial aerosol and total solar irradiance. Introducing the GLORY mission, Bull. Amer. Meteor. Soc.,80: 2229–2259, doi: http://dx.doi.org/10.1175/BAMS-88-5-677, 2007b.

O'Neill, N. T., Dubovik, O., and Eck, T. F.: Modified Ångström coefficient for the characterization of submicrometer aerosols, Appl. Opt., 40 (15), 2368–2375, doi: 10.1364/AO.40.002368, 2001.

O'Neill, N. T., Eck, T. F., Smirnov, A., Holben, B. N., and Thulasiraman, S.: Spectral discrimination of coarse and fine mode optical depth, J. Geophys. Res., 108 (D17), 4559–4573, doi:10.1029/2002JD002975, 2003.

Pandithuai, G., Dipu, S., Dani, K. K., Tiwari, S., Bisht, D. S., Devara, P. C. S., and Pinker, R. T.: Aerosol radiative forcing during dust events over New Delhi, India, J. Geophys. Res., 113, D13209, http://doi.org/10.1029/2008/D009804, 2008.

Pathak, B., Bhuyan, P. K., Gogoi, M. M., and Bhuyan, K.: Seasonal heterogeneity in aerosol types over Dibrugarh, North – Eastern India, Atmos. Env., 47, 307–315, doi: 10.1016/j.atmosenv.2011.10.061, 2012.

Pathak, B., Kalita, G., Bhuyan, P., and Moorthy, K.: Aerosol temporal characteristics and its impact on short wave radiative forcing at a location in the northeast of India, J. Geophys. Res., 115, D19204, http://dx.doi.org/10.10219/2009JD013462, 2010.

Ramachandran, S., and Cherian, R.: Regional and seasonal variations in aerosol optical characteristics and their frequency distributions over India during 2001–2005, J. Geophys. Res., 113, D08207, doi: 10.1029/2007JD008560, 2008.

Remer, L. A., Kaufman, Y. J., Tanré, D., Mattoo, S., Chu, D. A., Martins, J. V., Li, R. -R., Ichoku, C., Levy, R. C., Kledman, R. G., Eck, T. F., Vermote, E., and Holben, B. N.: The MODIS aerosol algorithm, products, and validation, J. Atmos. Sci., 62, 947−973, doi:10.1175/JAS3385.1, 2005.

Russell, P. B., Bergstrom, R. W., Shinozuka, Y., Clarke, A. D., DeCarlo, P. F., Jimenez, J. L., Livingston, J. M., Redemann, J., Dubovik, O., and Strawa, A.: Absorption Angstrom Exponent in AERONET and related data as an indicator of aerosol composition, Atmos. Chem. Phys., 10, 1155–1169, 2010.

Schmid, J., Michalsky, J. J., Slater, D. W., Bernard, J. C., Halthore, R. N., Liljegren, J. C., Holben, B. N., Eck, T. F., Livingston, J. M., Russell, J. B., Ingold, T., and Slustsker, I.: Comparison of columnar water-vapor measurements from solar transmittance methods, Appl. Opt., 40, 1886–1896, doi:10.1364/AO.40001886, 2001.

Schuster, G. L., Dubovik, O., and Holben, B. N.: Angstrom exponent and bimodal aerosol size distributions, J. Geophys. Res. Atmos., 111(D7), doi:10.1029/2005JD006328, 2006.

Singh, R. P., Dey, S., Tripathi, S. N., Tare, V., and Holben, B. N.: Variability of aerosol parameters over Kanpur, Northern India, J. Geophys. Res., 109, D23206, doi:10.1029/2004JD004966, 2004.

Sinha, P. R., Kaskaoutis, D. G., Manchanda, R. K., and Sreenivasan, S.: Characteristics of aerosols over Hyderabad, in Southern Peninsular India with the use of different techniques, Ann. Geophys., 30, 1393–1410, 2012.

Sinyuk, A., Torres, O., and Dubovik, O.: Combined use of satellite and surface observations to infer the imaginary part of the refractive index of Saharan dust, Geophys. Res. Lett., 30(2), 1081, doi:10.1029/ 2002GL016189, 2003.

Sinyuk, A., Dubovik, O., Holben, B. N., Eck, T. F., Breon, F-M., Martonchik, J., Khan, R., Diner, D. J., Verrmote, E. F., Roger, J. -C., Lapyonok, T., and Ilya, S.: Simultaneous retrieval of aerosol and surface properties from a combination of AERONET and satellite data, Remote Sens. Environ.,107, 90–108, 2007.

Smirnov, A., Holben, B. N., Eck, T. F., Dubovik, O., and Slutsker, I.: Cloud screening and quality control algorithms for the AERONET data base, Remote Sens. Environ., 73, 337–349, 2000.

Smirnov, A., Holben, B. N., Dubovic, O, O'Neill, N. T., Eck, T. F., Westphal, D. L., Goroth, A. K., Pietras, C., and Slutsker, I.: Atmospheric aerosol optical properties in the Persian Gulf, J. Atmos. Sci., 59, 620–634, doi:10.1175/1520-0469(2002)059<0620:AAOPIT>2.0CO; 2002a.

Smirnov, A., Holben, B. N., Kaufman, Y. J., Dubovic, O., Eck, T. F., Slutsker, I., Pietras, C., and Halthore, R. N.: Optical properties of atmospheric aerosol in maritime environments, J. Atmos. Sci., 59, 501–523, doi:10.1175/1520-0469(2002)059<0501:OPOAAI>2.0.CO; 2002b.

Smirnov, A., Holben, B. N., Lyapustin, A., Slutsker, I., and Eck, T. F.: AERONET processing algorithms refinement. Paper presented at AERONET Workshop, NASA-GSFC Aeronet Project, El Arenosillo, Spain, 10-14 May 2004, 2004.

Streets, D. G., Yan, F., Chin, M., Diehl, T., Mahowald, N., Schultz, M., Wild, M., Wu, Y., and Yu, C.: Anthropogenic and natural contributions to regional trends in aerosol optical depth, 1980–2006, J. Geophys. Res., 114, D00D18, doi:10.1029/2008JD011624, 2009.

Tanré, D., Bréon, F. M., Deuzé, J. L., Herman, M., Goloub, P., Nadal, F., and Marchand, A.: Global observation of anthropogenic aerosols from satellite, Geophy. Res. Lett., 28(24), 4555–4558, 2001.

Tan, H., Liu, L., Fan, S., Li, F., Yin, Y., Cai, M., and Chan, P. W.: Aerosol optical properties and mixing state of black carbon in the Pearl River Delta, China, Atmos. Environ., 131, 196–208, 2016.

Tiwari, S., Kaskaoutis, D., Soni, V. K., Attri, S. D., and Singh, A. K.: Aerosol columnar characteristics and their heterogeneous nature over Varanasi, in the central Ganges valley, Environ. Sci. Pollution Res., https://doi.org/10.1007/s11356-018-2502-4, 2018.

Tripathi, S., Dey, S., Chandel, A., Srivastava, A., Singh, R. P., and Holben, B. N.: Comparison of MODIS and AERONET derived aerosol optical depth over the Ganga basin, India, Annales Geophysicae, 23, 1093–1101, doi:10.5194/angeo-23-1093–2005, 2005.

Verma, S., Prakash, D., Ricaud, P., Payra, S., Jean-Luc Attie, and Soni, M.: A new classification of aerosol sources and types as measured over Jaipur, India, Aerosol and Air Qual. Res., 15, 985–993, 2015.

Vijayakumar, K., Devara, P. C. S., and Simha, C. P.: Aerosol features during drought and normal monsoon years: A study undertaken with multi-platform measurements over a tropical urban site. Aerosol and Air Qual. Res., 12, 1444–1458, doi: 10.4209/aaqr.2012.01.0005, 2012.

Vijayakumar, K., and Devara, P. C. S.: Variations in aerosol optical and microphysical properties during an Indian festival observed with space-borne and ground-based observations, Atmósfera, 25(4), 381–395, 2012.

Vijayakumar, K., and Devara, P. C. S.: Study of aerosol optical depth, ozone, and precipitable water vapour content over Sinhagad, a high-altitude station in the Western Ghats, Int. J. Remote Sens., 34(2), 613–630, 2013.

Vijayakumar, K., Devara, P. C. S., and Sonbawne, S. M.: Type-segregated aerosol effects on regional monsoon activity: A study using ground-based experiments and model simulations, Atmos. Environ., 99, 650–659, 2014.

Wang, M., Zhang, R., and Pu, Y.: Recent researches on aerosol in China. Adv. Atmos. Sci.,18,576–586, 2001.

Wild, M., Trüssel, B., Ohmura, A., Long, C. N., König-Langlo, G., Dutton, E. G., and Tsvetkov, A.: Global dimming and brightening: An update beyond 2000, J. Geophys. Res., 114, D00D13, doi:10.1029/2008JD011382, 2009.

Wu, L., and Zeng, Q-C.: Study on probability distributions of multi-timescale aerosol optical depth using AERONET data, Atmos. Ocean. Sci. Lett., 4, 216–222, 2011.

WMO.: Radiation Commission of IAPAM Meeting of Experts on Aerosol and Their Climatic Effects, pp. 28–30, WCP55, Williamsburg, VA, 1983.

Xia, X.: Parameterization of clear-sky surface irradiance and its implications for estimation of aerosol direct radiative effect and aerosol optical depth, Sci. Rep., 5, 14376, doi: 10.1038/srep14376, 2015.

Xie, Y., Li, Z., and Li, L.: Aerosol optical, microphysical, chemical and radiative properties of high aerosol load cases over the Arctic based on AERONET measurements, Sci. Rep., 8, 9376, http://doi.org/10.1038/s41598-018-27744-z, 2018.

Yu, H., Kaufman, Y. J., Chin, M., Feingold, G., Remer, L. A., Anderson, T. L., Balkanski, Y., Bellouin, N., Boucher, O., Christopher, S., Decola, P., Kahn, R., Koch, D., Loeb, N., Reddy, M. S., Schulz, M., Takemura, T., and Zhou, M.: A review of measurement-based assessments of aerosol direct radiative effect and forcing, Atmos. Chem. Phys., 6, 613–666, doi: 10.5194/acp-6-613-2006, 2006.

Zege, E. P., Ivanov, A. P., and Katzev, I. L.: Image transfer through a scattering medium, Springer, Berlin, New York, USA, 1991.

Zhao, T. X., Laszlo -P. I., Guo, W., Heidinger, A., Cao, C., Jelenak, A., Tarpley, D., and Sullivan, J.: Study of long-term trend in aerosol optical thickness observed from operational AVHRR satellite instrument, J. Geophys. Res., 113, D07201, doi:10.1029/2007JD009061, 2008.